A Detailed Analysis of Beam Formation with Electron Guns of the Pierce Type

By W. E. DANIELSON, J. L. ROSENFELD,* and J. A. SALOOM

(Manuscript received November 10, 1955)

The theory of Cutler and Hines is extended in this paper to permit an analysis of beam-spreading in electron guns of high convergence. A lens correction for the finite size of the anode aperture is also included. The Cutler and Hines theory was not applicable to cases where the effects of thermal velocities are large compared with those of space charge and it did not include a lens correction. Gun design charts are presented which include all of these effects. These charts may be conveniently used in choosing design parameters to produce a prescribed beam.

CONTENTS

---

* Mr. Rosenfeld participated in this work while on assignment to the Laboratories as part of the M.I.T. Cooperative Program.

GLOSSARY OF SYMBOLS

$A_{1,2}$	anode designations
B, C	anode potentials
$C_{1,2}$	functions used in evaluating σ_+'
dA	increment of area
dl, dz	increments of length
e	electronic charge, base of natural logarithms
E_n	electric field normal to electron path
F	modified focal length of the anode lens
F_D	focal length of the anode lens as given by Davisson[4]
F_n	force acting normal to an electronic path
$F_{r,\sigma}$	fraction of the total current which would flow through a circle of radius r, σ
I, I_D	total beam current
I_r	beam current within a radius, r, of the center
J	current density
k	Boltzman's constant
K	a quantity proportional to gun perveance
m	electronic mass
P	gun perveance
$P(r)$	probability that a thermal electron has a radial position between r and $r + dr$
r	radial distance from beam axis
$r_{a,c}$	anode, cathode radii
r_e	distance from beam axis to path of an electron emitted with zero velocity at the edge of the cathode
r_{95}	radius of circle through which 95% of the beam current would pass
$\bar{r}$	distance from center of curvature of cathode; hence, $\bar{r}_c$ is the cathode radius of curvature and $(\bar{r}_c - \bar{r}_a)$ is the distance from cathode to anode
r_{e^+}'	slope of edge nonthermal electron path on drift side of enode lens
r_{e^-}'	slope of edge nonthermal electron path on gun side of anode lens
R	a dummy integration variable
t	time
T	cathode temperature in degrees K
u	longitudinal electron velocity
$v_{c,x,y}$	transverse electron velocities
$V, V_{a,f,x}$	beam voltages with cathode taken as ground

$V(\bar{r}, r)$, $V_c(\bar{r}, r)$, etc.	potential distributions used in the anode lens study
V'	voltage gradient
z	distance along the beam from the anode lens
$z_{\min}$	distance to the point where r_{95} is a minimum
$(-\alpha)$	Langmuir potential parameter for spherical cathode-anode gun geometry
γ	slope of an electron's path after coming into a space charge free region just beyond the anode lens
Γ	the factor which divides F_D to give the modified anode focal length
δ	dimensionless radius parameter
ϵ_0	dielectric constant of free space
ζ	dimensionless voltage parameter
θ	slope of an electron's path in the gun region
η	charge to mass ratio for the electron
μ	normalized radial position in a beam
σ	the radial position of an electron which left the cathode center with "normal" transverse velocity
σ_+'	slope of σ-electron on drift side of anode lens
σ_-'	slope of σ-electron on gun side of anode lens
ψ	electric flux

1. INTRODUCTION

During the past few years there have been several additions to the family of microwave tubes requiring long electron beams of small diameter and high current density. Due to the limited electron current which can be drawn from unit area of a cathode surface with some assurance of long cathode operating life, high density electron beams have been produced largely through the use of convergent electron guns which increase markedly the current density in the beam over that at the cathode surface.

An elegant approach to the design of convergent electron guns was provided by J. R. Pierce[1] in 1940. Electron guns designed by this method are known as *Pierce guns* and have found extensive use in the production of long, high density beams for microwave tubes.

More recent studies, reviewed in Section 2, have led to a better understanding of the influence on the electron beam of (a) the finite velocities with which electrons are emitted from the cathode surface, and (b) the defocusing electric fields associated with the transition from the accelerating region of the gun to the drift region beyond. Although these two effects have heretofore been treated separately, it is in many cases

necessary to produce electron beams under circumstances where both effects are important and so must be dealt with simultaneously and more precisely than has until now been possible. It is the purpose of this paper to provide a simple design procedure for typical Pierce guns which includes both effects. Satisfactory agreement has been obtained between measured beam contours and those predicted for several guns having perveances (i.e., ratios of beam current to the $\frac{3}{2}$ power of the anode voltage) from 0.07×10^{-6} to 0.7×10^{-6} amp $(\text{volt})^{-3/2}$.

2. PRESENT STATUS OF GUN DESIGN — LIMITATIONS

Gun design techniques of the type originally suggested by J. R. Pierce were enlarged in papers by Samuel[2] and by Field[3] in 1945 and 1946. Samuel's work did not consider the effect of thermal velocities on beam shape and, although Field pointed out the importance of thermal velocities in limiting the theoretically attainable current density, no method for predicting beam size and shape by including thermal effects was suggested. The problem of the divergent effect of the anode lens was treated in terms of the Davisson[4] electrostatic lens formula, and no corrections were applied.*

More recently, Cutler and Hines[6] and also Cutler and Saloom[7] have presented theoretical and experimental work which shows the pronounced effects of the thermal velocity distribution on the size and shape of beams produced by Pierce guns. Cutler and Saloom also point to the critical role of the beam-forming electrode in minimizing beam distortion due to improper fields in the region where the cathode and the beam-forming electrode would ideally meet. With regard to the anode lens effect, these authors also show experimental data which strongly suggest a more divergent lens than given by the Davisson formula. The Hines and Cutler thermal velocity calculations have been used[6, 7] to predict departures in current density from that which should prevail in ideal beams where thermal electrons are absent. Their theory is limited, however, by the assumption that the beam-spreading caused by thermal velocities is small compared to the nominal beam size.

In reviewing the various successes of the above mentioned papers in affording valuable tools for electron beam design, it appeared to the present authors that significant improvement could be made, in two respects, by extensions of existing theories. First, a more thorough in-

* It is in fact erroneously stated in Reference 5 that the lens action of an actual structure must be somewhat weaker than predicted by the Davisson formula so that the beam on leaving the anode hole is more convergent than would be calculated by the Davisson method. This question is discussed further in Section 3.

vestigation of the anode lens effect was called for; and second, there was a need to extend thermal velocity calculations to include cases where the percentage increase in beam size due to thermal electrons was as large as 100 per cent or 200 per cent. Some suggestions toward meeting this second need have been included in a paper by M. E. Hines.[8] They have been applied to two-dimensional beams by R. L. Schrag.[9] The particular assumptions and methods of the present paper as applied to the two needs cited above are somewhat different from those of References 8 and 9, and are fully treated in the sections which follow.

3. TREATMENT OF THE ANODE LENS PROBLEM

Using thermal velocity calculations of the type made in Reference 6, it can easily be shown that at the anode plane of a typical moderate perveance Pierce type electron gun, the average spread in radial position of those electrons which originate from the same point of the cathode is several times smaller than the beam diameter. For guns of this type, then, we may look for the effect of the anode aperture on an electron beam for the idealized case in which thermal velocities are absent and confidently apply the correction to the anode lens formula so obtained to the case of a real beam.

Several authors have been concerned with the diverging effect of a hole in an accelerating electrode where the field drops to zero in the space beyond,[10] but these treatments do not include space charge effects except as given by the Davisson formula for the focal length, F_D, of the lens:

$$F_D = -\frac{4V}{V'} \tag{1}$$

where V' would be the magnitude of the electric field at the aperture if it were gridded, and V would be the voltage there.

In attempting to describe the effect of the anode hole with more accuracy than (1) affords, we have combined analytical methods with electrolytic tank measurements in two rather different ways. The first method to be given is more rigorous than the second, but a modification of the second method is much easier to use and gives essentially the same result.

A. Superposition Approach to the Anode Lens Problem

Special techniques are required for finding electron trajectories in a space charge limited Pierce gun having a non-gridded anode. M. E.

Hines has suggested* that a fairly accurate description of the potential distribution in such guns can be obtained by a superposition method as follows:

By the usual tank methods, find suitable beam forming electrode and anode shapes for conical space charge limited flow in a diode having cathode and anode radii of curvature given by $\bar{r}_c$ and $\bar{r}_{a1}$, respectively, as shown in Fig. 1(a). Using the electrolytic tank with an insulator along the line which represents the beam edge, trace out an equipotential which intersects the insulator at a distance $\bar{r}_{a2}$ from the cathode center of curvature. Let the cathode be at ground potential and let the voltage on anode A_1 be called B. Suppose, now, that we are interested in electron trajectories in a non-gridded gun where the edge of the anode hole is a distance $\bar{r}_{a2}$ from the center of curvature of the cathode. Let the voltage, C, for this anode be chosen the same as the value of the equipotential traced out above for the case of cathode at ground potential and A_1 at potential B. If we consider the space charge limited flow from a cathode which is followed by the apertured anode, A_2, and the full anode, A_1, at potentials C and B, respectively, it is clear that a conical flow of the type which would exist between concentric spheres will result. The flow for such cases was treated by Langmuir,[14] and the associated potentials are commonly called the "Langmuir potentials."

If we operate both A_1 and A_2 at potential C, however, the electrons will pass through the aperture in anode A_2 into a nearly field-free region. If the distance, $\bar{r}_{a2} - \bar{r}_{a1}$, from A_2 to A_1 is greater than the diameter of the aperture in A_2, the flow will depend very little on the shape of A_1 and the electron trajectories and associated equipotentials will be of the type we wish to consider except in a small region near A_1. We will shortly make use of the fact that the space charge between cathode and A_2 is not changed much when the voltage on A_1 is changed from B to C, but first we will define a set of potential functions which will be needed.

In order to obtain the potential at arbitrary points in any axially symmetric gun when space charge is not neglected, we may superpose potential solutions to 3 separate problems where, in each case, the boundary condition that each electrode be an equipotential is satisfied. We will follow the usual notation in using $\bar{r}$ for the distance of a general point from the cathode center of curvature, and r for its radial distance from the axis of symmetry. Let $V_a(\bar{r}, r)$, $V_b(\bar{r}, r)$ and $V_{sc}(\bar{r}, r)$ be the three potential solutions where: (1) $V_a(\bar{r}, r)$ is the solution for the case of no space charge with A_1 and cathode at zero potential and A_2 at potential C, (2) $V_b(\bar{r}, r)$ is the solution for the case of no space charge with A_2

* Verbal disclosure.

and cathode at zero potential and A_1 at potential B, and (3) $V_{sc}(\bar{r}, r)$ is the solution when space charge is present but when A_1, A_2, and cathode are all grounded.

If the configuration of charge which contributes to $V_{sc}(\bar{r}, r)$ is that corresponding to ideal Pierce type flow, then we can use the principle of superposition to give the Langmuir potential, $V_L(\bar{r}, r)$:

$$V_L(\bar{r}, r) = V_a(\bar{r}, r) + V_b(\bar{r}, r) + V_{sc}(\bar{r}, r) \tag{2}$$

Furthermore, the potential configuration for the case where A_1 and A_2 are at potentical C can be written

$$V = V_a + \frac{C}{B} V_b + V_{(sc)'} \tag{3}$$

where the functional notation has been dropped and $V_{(sc)'}$ is the po tential due to the new space charge when A_1 and A_2 are grounded. We are now ready to use the fact that $V_{(sc)'}$ may be well approximated by V_{sc} which is easily obtained from (2). This substitution may be justified by noting that the space charge distribution in a gun using a voltage C for A_1 does not differ significantly from the corresponding distribution when A_1 is at voltage B except in the region near and beyond A_2 where the charge density is small anyway (because of the high electron velocities there). Substituting V_{sc} as given by (2) for $V_{(sc)'}$ in (3) then gives

$$V \approx V_L - \left(1 - \frac{C}{B}\right) V_b \tag{4}$$

We have thus obtained an expression, (4), for the potential at an arbi-

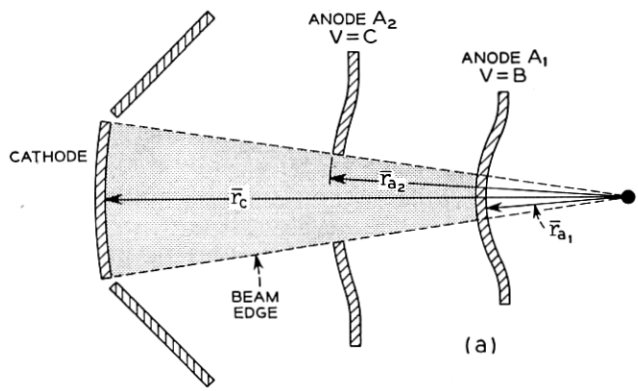

Fig. 1(a) — Electrode configuration for anode lens evaluation in Section 3A.

trary point in our gun in terms of the well known solution for space charge limited flow between two concentric spheres, V_L, and a potential distribution, V_b, which does not depend on space charge and can therefore be obtained in the electrolytic tank. Once the potential distribution is found, electron trajectories may be calculated, and an equivalent lens system found. Equation (4) is used in this way in Part C as one basis for estimating a correction to the Davisson equation. (It will be noted that (4) predicts a small but finite negative field at the cathode. This is because the space charge density associated with V_{sc} is slightly greater near the cathode than that associated with $V_{(sc)'}$, and it is this latter space charge which will make the field zero at the cathode under real space charge limited operation. Equation (4), as applied in Part C of this section, is used to give the voltage as a function of position at all points except near the cathode where the voltage curves are extended smoothly to make the field at the cathode vanish.)

B. Use of a False Cathode in Treating the Anode Lens Problem

Before evaluating the lens effect by use of (4), it will be useful to develop another approach which is a little simpler. The evaluation of the lens effect predicted by both methods will then be pursued in Part C where the separate results are compared.

In Part A we noted that no serious error is made in neglecting the difference between the two space charge configurations considered there because these differences were mainly in the very low space charge region near and beyond A_2. It similarly follows that we can, with only a small decrease in accuracy, ignore the space charge in the region near and beyond A_2 so long as we properly account for the effect of the high space charge regions closer to the cathode. To place the foregoing observations on a more quantitative basis, we may graph the Langmuir potential (for space charge limited flow between concentric spheres) versus the distance from cathode toward anode, and then superpose a plot of the potential from LaPlace's equation (concentric spheres; no space charge) which will have the same value and slope at the anode. The LaPlace curve will depart significantly from the Langmuir in the region of the cathode, but will adequately represent it farther out.[11] Our experience has shown that the representation is "adequate" until the difference between the two potentials exceeds about 2 per cent of the anode voltage. Then, since space charge is not important in the region near the anode for the case of a gridded Pierce gun, corresponding to space charge limited flow between concentric spheres, it can be expected to be similarly unimportant for cases where the grid is replaced by an aperture. Let us

therefore consider a case where electrons are emitted perpendicularly and with finite velocity from what would be an appropriate spherical equipotential between cathode and anode in a Pierce type gun. So long as (a) there is good agreement between the LaPlace and Langmuir curves at this artificial cathode and (b) the distance from this artificial cathode to the anode hole is somewhat greater than the hole diameter, we will find that the divergent effect of the anode hole will be very nearly the same in this concocted space charge free case as in the actual case where space charge is present. (The quantitative support for this last statement comes largely from the agreement between calculations based on this method and calculations by method A.) The electrode configuration is shown in Fig. 1(b), and the potential distribution in this space charge free anode region can now be easily obtained in the electrolytic tank. This potential distribution will be used in the next section to provide a second basis for estimating a correction to the Davisson equation.

C. Calculation of Anode Lens Strength by the Two Methods

The Davisson equation, (1), may be derived by assuming that none of the electric field lines which originate on charges in the cathode-anode region leave the beam before reaching the ideal anode plane where the voltage is V, and that all of these field lines leave the beam symmetrically and radially in the immediate neighborhood of the anode. Electrons are thus considered to travel in a straight line from cathode to anode, and then to receive a sudden radial impulse as they cross radially diverging electric field lines at the anode plane. A discontinuous change in

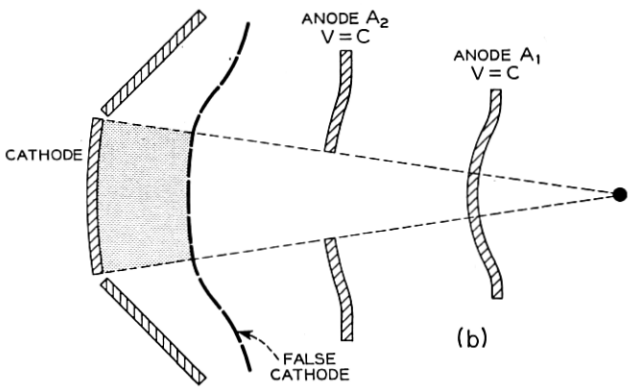

Fig. 1(b) — The introduction of a false cathode at the appropriate potential allows the effect of space charge on the potential near the anode hole to be satisfactorily approximated as discussed in Section 3*B*.

slope is therefore produced as is common to all thin lens approximations. The diverging effect of electric field lines which originate on charges which have passed the anode plane is then normally accounted for by the universal beam spread curve.[12] In our attempt to evaluate the lens effect more accurately, we will still depend upon using the universal beam spread curve in the region following the lens and on treating the equivalent anode lens as thin. Consequently our improved accuracy must come from a mathematical treatment which allows the electric field lines originating in the cathode-anode region to leave the beam gradually, rather than a treatment where all of these flux lines leave the beam at the anode plane. In practice the measured perveances, $P(= I/V^{3/2})$, of active guns of the type considered here have averaged within 1 or 2 per cent of those predicted for corresponding gridded Pierce guns. Therefore the total space charge between cathode and anode is much the same with and without the use of a grid, even though the charge distribution is not the same in the two cases. The total flux which must leave our beam is therefore the same as that which will leave the corresponding idealized beam and we may write

$$\psi = \int E_n \, dA = \pi r_a^2 V_{\text{ideal}}' \tag{5}$$

where E_n is the electric field normal to the edge of the beam, $r_a = r_c(\bar{r}_a/\bar{r}_c)$ is the beam radius at the anode lens, and V_{ideal}' is the magnitude of the field at the corresponding gridded Pierce gun anode.

To find the appropriate thin lens focal length we will now find the total integrated transverse impulse which would be given to an electron which follows a straight-line path on both sides of the lens (see Fig. 2), and we will equate this impulse to $m\Delta u$ where Δu is the transverse velocity given to the electron as it passes through the equivalent thin lens. In this connection we will restrict our attention to paraxial electrons and evaluate the transverse electric fields from (4) and from the tank plot outlined in Section B, respectively. The total transverse impulse experienced by an electron can be written

$$\int_{\text{Path}} F_n \, dt = e \int_{\text{Path}} \frac{E_n}{u} \, dl \tag{6}$$

where u is the velocity along the path and F_n is the force normal to the path.

We will usually find that the correction to (1) is less than about 20 per cent. It will therefore be worthwhile to put (6) in a form which in effect allows us to calculate *deviations* from F_D as given by (1) instead

of deriving a completely new expression for F. In accomplishing this purpose, it will be helpful to define a dimensionless function of radius, δ, by

$$\frac{r_a}{r} = 1 + \delta, \tag{7a}$$

and a dimensionless function of voltage, ζ, by

$$\sqrt{\frac{V_x}{V}} = 1 + \zeta, \tag{7b}$$

where r_a is the radius at the anode lens when the lens is considered thin, and V_x is a constant voltage to be specified later. (Note that the quantities δ and ζ are not necessarily small compared to 1.) Using $u = \sqrt{2\eta V}$, and substituting for $\sqrt{V}$ from (7b) we obtain

$$e\int \frac{E_n\, dl}{u} = \frac{4}{r_a\sqrt{2\eta V_x}}\int E_n r(1 + \zeta + \delta + \zeta\delta)\, dl \tag{8}$$

where use has also been made of (7a) in the form $1 \equiv r(1 + \delta)/r_a$. Now, as outlined above, we equate this impulse to $m\Delta u$, and we obtain

$$\Delta u = \frac{e/m}{r_a\sqrt{2\eta V_x}}\left(\int E_n r\, dl + \int E_n r(\zeta + \delta + \zeta\delta)\, dl\right) \tag{9}$$

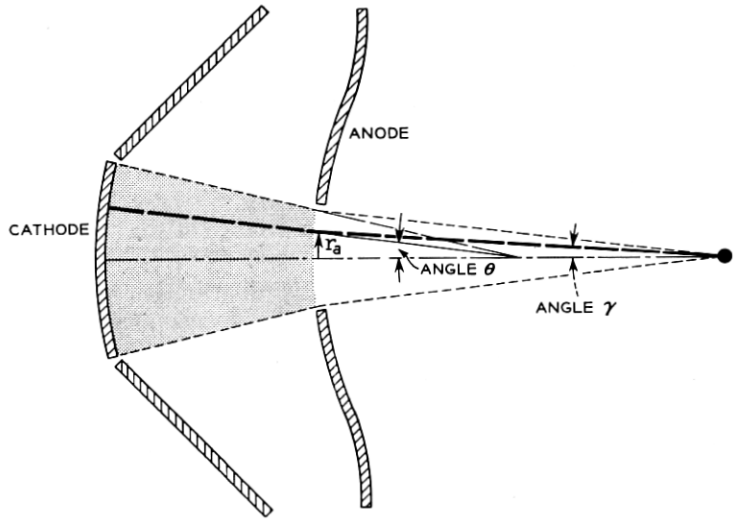

Fig. 2 — The heavy line represents an electron's path when the effect of the anode hole may be represented by a thin lens, and when space charge forces are absent in the region following the anode aperture. For paraxial electrons, the (negative) focal length is related to the indicated angles by ($\gamma = \theta + r_a/F$).

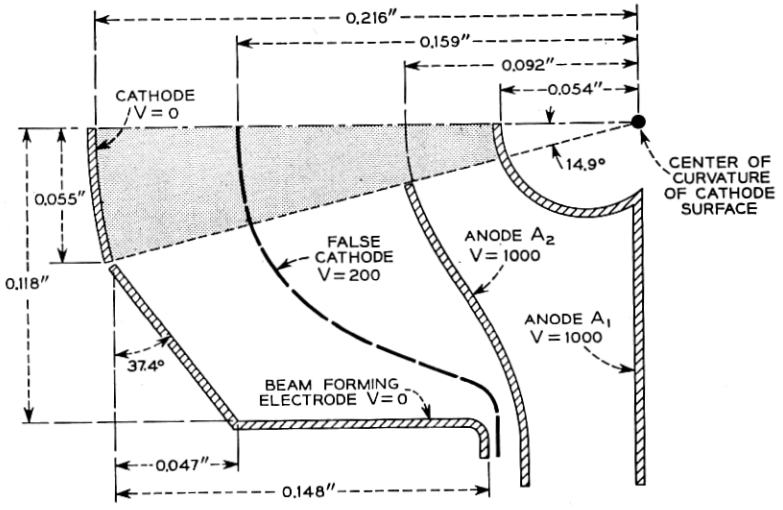

Fig. 3 — The gun parameters used in Section 3*C* for comparing two methods of evaluating the effect of the anode lens.

The first integral can be obtained from (5); hence, if we are able to choose V_x so that the second integral vanishes, we may write:

$$\Delta u = \frac{\eta}{r_a\sqrt{2\eta V_x}}\left(\frac{r_a^2 V_{\text{ideal}}'}{2}\right)$$

The reciprocal of the thin lens focal length is therefore

$$\frac{1}{F} = -\frac{\Delta u}{r_a u_f} = -\frac{V'}{4\sqrt{V_x V_f}} \tag{10}$$

where u_f and V_f are the final velocity and voltage of the electron after it leaves the lens region.

The real task, then, is to use the potential distribution in the gun as obtained by the methods of Part *A* or Part *B* above to find the value of V_x which causes the last integral in (9) to vanish: To compare the two focal lengths obtained by the methods of Part *A* and *B* respectively, a specific tank design of the type indicated in Fig. 1 was carried out. The relevant gun parameters are indicated in Fig. 3. Approximate voltages on and near the beam axis were obtained as indicated in Parts *A* and *B*, above, with the exception that in the superposition method, A, special techniques were used to subtract the effect of the space charge lying in the post-anode region (because the effect of this space charge is accounted for separately as a divergent force in the drift region*). From these data,

* See Section 4B.

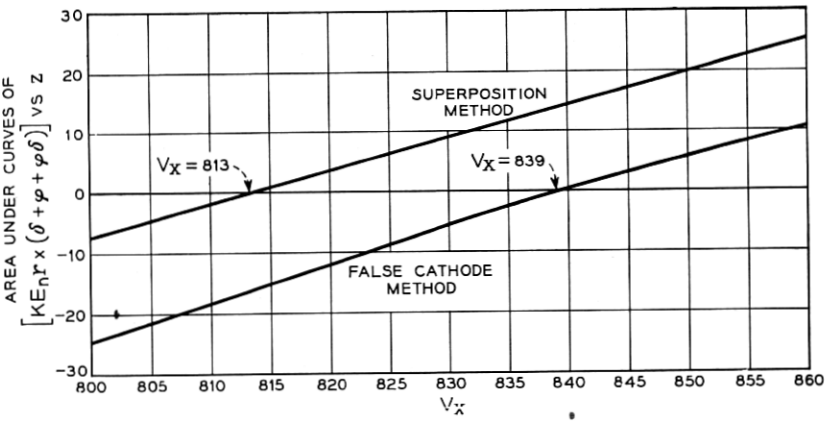

Fig. 4 — Curves for finding the value of V_x to be used in equation (10) for the set of gun parameters of Fig. 3.

both the direction and magnitude of the total electric field near the beam axis were (with much labor) determined. Once these data had been obtained, a trial value was selected for V_x, and the corresponding focal length was calculated by (10). This enabled the electron's path through the associated thin lens to be specified so that, at this point in the procedure, both r and V were known functions of ℓ, and the quantities δ and ζ were then obtained as functions of ℓ from (7). Finally the second integral in (9) was evaluated for the particular V_x chosen, and then the process was repeated for other values of V_x. Fig. 4 shows curves whose ordinates are proportional to this second integral and whose abscissae are trial values for V_x. As noted above, the appropriate value for V_x is that value which makes the ordinate vanish, so that we obtain $V_x = 813$ and 839 for methods A and B, respectively. The percentage difference in the focal lengths obtained by the two methods is thus only 1.6 per cent, and the reasonableness of making calculations as outlined in Part *B* is thus put on a more quantitative basis.

Even calculations based on the method of Part *B* are tedious, and we naturally look for simpler methods of estimating the lens effect. In this connection we have found that V_x is usually well approximated by the value of the potential at the point of intersection between the beam axis and the ideal anode sphere. The specific values of the potential at this point as obtained by the methods of Parts *A* and *B* were 814 and 827, respectively. It will be noted that these values agree remarkably well with the values obtained above. Furthermore, very little extra effort is required to obtain the potential at this intersection in the false cathode case:

Electrolytic tank measurements are normally made in the cathode-anode region to give the potential variation along the outside edge of the electron beam (for comparison with the Langmuir potential); hence, by tracing out a suitable equipotential line, the shape of the false cathode can easily be obtained. With the false cathode in place and at the proper potential, the approximate value for V_x is then obtained by a direct tank measurement of the potential at an axial point whose distance from the true cathode center is $(\bar{r}_c - \bar{r}_a)$ as outlined above. Although finite electron emission velocities typically do not much influence the trajectory of an electron at the anode, they do nevertheless significantly alter the beam in the region beyond. It is in this affected region where experimental data can be conveniently taken. We must, therefore, postpone a comparison of lens theory with experiment until the effect of thermal velocities has been treated. At that time theoretical predictions combining the effects of both thermal velocities and the anode lens can be made and compared with experiment. Such a comparison is made in Section 6.

4. TREATMENT OF BEAM SPREADING, INCLUDING THE EFFECT OF THERMAL ELECTRONS

In Section 2 the desirability of having an approach to the thermal spreading of a beam which would be applicable under a wide variety of conditions was stressed. In particular, there was a need to extend thermal velocity calculations to include the effects of thermal velocities even when electrons with high average transverse velocities perturb the beam size by as much as 100 or 200 per cent. Furthermore, a realistic mathematical description which would allow electrons to cross the axis seemed essential. The method described below is intended adequately to answer these requirements.

A. The Gun Region

The Hines-Cutler[6] method of including the effect of thermal velocities on beam size and shape leads one to conclude that, for usual anode voltages and gun perveance, the beam density profile in the plane of the anode hole is not appreciably altered by thermal velocities of emission. (This statement will be verified and put on a more quantitative basis below.) Under these conditions, the beam at the anode is adequately described by the Hines-Cutler treatment. We will therefore find it convenient to adopt their notation where possible, and it will be worthwhile to review their approach to the thermal problem.

It is assumed that electrons are emitted from the cathode of a thermionic gun with a Maxwellian distribution of transverse velocities

$$dJ_c = J_c \frac{m}{2\pi kT} e^{-(m/2kT)(v_x^2+v_y^2)}\, dv_x\, dv_y \tag{11}$$

where J_c is the cathode current density in the z direction, T is the cathode temperature, and v_x and v_y are transverse velocities. The number of electrons emitted per second with radially directed voltages between V and $V + dV$ is then

$$dJ_c = J_c e^{-(Ve/kT)}\, d\left(\frac{Ve}{kT}\right) \tag{12}$$

Now in the accelerating region of an ideal Pierce gun (and more generally in any beam exhibiting laminar flow and having constant current density over its cross section) the electric field component perpendicular to the axis of symmetry must vary linearly with radius. Consequently Hines and Cutler measure radial position in the electron beam as a fraction, μ, of the outer beam radius (r_e) at the same longitudinal position,

$$r = \mu r_e \tag{13}$$

The laminar flow assumption for constant current densities and small beam angles implies a radius of curvature for laminar electrons which also varies linearly with radius at any given cross section so that

$$\frac{d^2r}{dt^2} = \mu \frac{d^2r_e}{dt^2} \tag{14}$$

Substituting for r from (13), (14) becomes

$$\frac{d^2\mu}{dt^2} + \left(\frac{2}{r_e}\frac{dr_e}{dt}\right)\frac{d\mu}{dt} = 0 \tag{15}$$

where r_e and dr/dt can be easily obtained from the ideal Langmuir solution. Since the equation is linear in μ, we are assured that the radial position of a non-ideal electron that is emitted with finite transverse velocity from the cathode center (where $\mu = 0$) will, at any axial point, be proportional to $d\mu/dt$ at the cathode.

Let us now define a quantity "σ" such that $\mu = \sigma/r_e$ is the solution to (15) with the boundary conditions $\mu_c = 0$ and

$$\left(\frac{d\mu}{dt}\right)_c = \frac{1}{r_c}\sqrt{\frac{kT}{m}}$$

where the subscript c denotes evaluation at the cathode surface, k is

Boltzman's constant, T is the cathode temperature in degrees Kelvin, and m is mass of the electron. For the case $\mu_c = 0$, but with arbitrary initial transverse velocity, we will then have

$$\mu = \frac{\sigma}{r_c} \frac{\left(\frac{d\mu}{dt}\right)_c}{\frac{1}{r_c}\sqrt{\frac{kT}{m}}} \tag{16}$$

Hence we can express σ in terms of the thermal electron's radial position (r), and its initial transverse velocity, v_c,

$$\sigma = \frac{\mu r_c \sqrt{\frac{kT}{m}}}{\left(\frac{d(\mu r_c)}{dt}\right)} \equiv \frac{r\sqrt{\frac{kT}{m}}}{v_c} \tag{17}$$

The quantity σ can now be related to the radial spread of thermal electrons (emitted from a given point on the cathode) with respect to an electron with no initial velocity: By (11) we see that the number of electrons leaving the cathode with $d\mu/dt = v_c/r_c$ is proportional to $v_c \exp -v_c^2 m/2kT$. Suppose many experiments were conducted where all electrons except one at the cathode center had zero emission velocity, and suppose the number of times the initial transverse velocity of the single thermal electron were chosen as v_c, is proportional to $v_c \exp -v_c^2 m/2kT$. Then the probability, $P(r)$, that the thermal electron would have a radial position between r and $r + dr$ when it arrived at the transverse plane of interest would be proportional to $v_c \exp -v_c^2(m/2kT)$. Here v_c is the proper transverse velocity to cause arrival at radius r, and by (17) we have

$$v_c = \frac{r}{\sigma}\sqrt{\frac{kT}{m}}$$

so that the probability becomes

$$P(r) = J_c e^{-(r^2/2\sigma^2)}\, d\left(\frac{r^2}{2\sigma^2}\right) \tag{18}$$

We therefore identify σ with the standard deviation in a normal or Gaussian distribution of points in two dimensions. At the real cathode, thermal electrons are simultaneously being emitted from the cathode surface with a range of transverse velocities. However, if σ as defined above is small in comparison with r_c, the forces experienced by a thermal electron when other thermal electrons are present will be very nearly

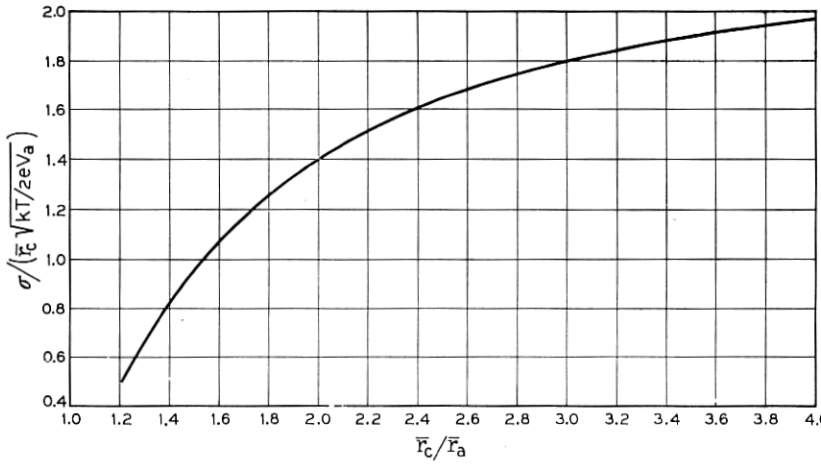

Fig. 5 — Curves useful in finding the transverse displacement of electron trajectories at the anode of Pierce-type guns.

the same as the forces involved in the equations above. Thus if $\sigma \ll r_e$, (18) may be taken as the distribution, in a transverse plane, of those electrons which were simultaneously emitted at the cathode center. Furthermore, the nature of the Pierce gun region is such that electrons emitted from any other point on the cathode will be similarly distributed with respect to the path of an electron emitted from this other point with zero transverse velocity (so long as they stay within the confines of the ideal beam). Hines and Cutler have integrated (15) with $\mu_c = 0$ and $(d\mu/dl)_c = 1$ to give $\sigma/(\bar{r}_c\sqrt{kT/2eV_a})$ at the anode as a function of $\bar{r}_c/\bar{r}_a$. This relationship is included here in graphical form as Fig. 5.

For a large class of magnetically shielded Pierce-type electron guns, including all that are now used in our traveling wave tubes, r_e/σ at the anode is indeed found to be greater than 5 (in most cases, greater than 10) so that evaluation of σ at the anode of such guns can be made with considerable accuracy by the methods outlined above. One source of error lies in the assumption that electrons which are emitted from a point at the cathode edge become normally distributed about the corresponding non-thermal (no transverse velocity of emission) electron's path, and with the same standard deviation as calculated for electrons from the cathode center. In the gun region where r_e/σ tends to be large this difference between representative σ-values for the peripheral and central parts of the beam is unimportant, but it must be re-examined in the drift region following the anode.

We have already investigated the region of the anode hole in some detail in Section 3 and have found it worth while to modify the ideal Davisson expression for focal length of an equivalent anode lens. In particular, let us define a quantity Γ by

$$F = \text{focal length} = F_D/\Gamma \tag{19}$$

where F_D is the Davisson focal length. Thus Γ represents a corrective factor to be applied to F_D to give a more accurate value for the focal length. In so far as any thin lens is capable of describing the effects of diverging fields in the anode region, we may then use the appropriate optical formulas to transfer our knowledge of the electron trajectories (calculated in the anode region as outlined above) to the start of the drift region. In particular,

$$\left(\frac{dr}{dz}\right)_2 = \left(\frac{dr}{dz}\right)_1 - \frac{r}{F} \tag{20}$$

where $(dr/dz)_1$ and $(dr/dz)_2$ are the slopes of the path just before and just after the lens, and r is the distance from the axis to the point where the ideal path crosses the lens plane.

B. The Drift Region

Although r_e/σ was found to be large at the anode plane for most guns of interest, this ratio often shrinks to 1 or less at an axial distance of only a few beam diameters from the lens. Therefore, the assumption that electron trajectories may be found by using the space charge forces which would exist in the absence of thermal velocities of emission (i.e., forces consistant with the universal beam spread curve) may lead to very appreciable error. For example, if equal normal (Gaussian) distributions of points about a central point are superposed so that the central points are equally dense throughout a circle of radius r_e, and if the standard deviation for each of the normal distributions is $\sigma = r_e$, the relative density of points in the center of the circle is only about 39 per cent of what it would be with $\sigma < (r_e/5)$.

In order to minimize errors of this type we have modified the Hines-Cutler treatment of the drift space in two ways: (1) The forces influencing the trajectories of the non-thermal electrons are calculated from a progressive estimation of the actual space charge configuration as modified by the presence of thermal electrons. (2) Some account is taken of the fact that, as the space charge density in the beam becomes less uniform as a function of radius, the spread of electrons near the center of the beam increases more rapidly than does the corresponding spread

farther out. Since item (1) is influenced by item (2), the specific assumptions involved in the latter case will be treated first.

When current density is uniform across the beam and its cross section changes slowly with distance, considerations of the type outlined above for the gun region show that those thermal electrons which remain within the beam will continue to have a Gaussian distribution with respect to a non-thermal electron emitted from the same cathode point. When current density is not uniform over the cross section, we would still like to preserve the mathematical simplicity of obtaining the current density as a function of beam radius merely by superposing Gaussian distributions which can be associated with each non-thermal electron. To lessen the error involved in this simplified approach, we will arrive at a value for the standard deviation, σ (which specifies the Gaussian distribution), in a rather special way. In particular, σ at any axial position, z, will be taken as the radial coordinate of an electron emitted from the center of the cathode with a transverse velocity of emission given by,

$$v_c = \sqrt{\frac{kT}{m}} \tag{21}$$

It is clear from (17) that for such an electron, $r = \sigma$ in the gun region. From (18), the fraction of the electrons from a common point on the cathode which will have $r \leqq \sigma$ in the gun region is

$$\text{fraction} = \int_0^{\sigma} e^{-(r^2/2\sigma^2)}\, d\,\frac{r^2}{2\sigma^2} = 1 - e^{-1/2} = 0.393 \tag{22}$$

If r_e denotes the radial position of the outermost non-thermal electron and if $\sigma > r_e$, the "σ-electron" will be moving in a region where the space charge density is significantly lower than at the axis. We could, of course, have followed the path of an electron with initial velocity equal to say 0.1 or 10 times that given in (21) and called the corresponding radius 0.1σ or 10σ. The reason for preferring (21) is that about 0.4 or nearly half of the thermal electrons emitted from a common cathode point will have wandered a distance less than σ from the path of a non-thermal electron emitted from the same cathode point, while other thermal electrons will have wandered farther from this path; consequently, the current density in the region of the σ-electron is expected to be a reasonable average on which beam spreading due to thermal velocities may be based. With this understanding of how σ is to be calculated, we can proceed to the calculation of non-thermal electron trajectories as suggested in item (1).

The non-thermal paths remain essentially laminar, and with r_e denoting the radial coordinate of the outermost non-thermal electron, we will make little error in assuming that the current density of non-thermal electrons is constant for $r < r_e$. Consequently, if equal numbers of thermal electrons are assumed to be normally distributed about the corresponding non-thermal paths, the longitudinal current density as a function of radius can be found in a straightforward way[13] by using (18). The result is

$$\frac{J_r}{J_D} = e^{-(r^2/2\sigma^2)} \int_0^{r_e/\sigma} \frac{R}{\sigma} e^{-(R^2/2\sigma^2)} I_0\left(\frac{rR}{\sigma^2}\right) d\left(\frac{R}{\sigma}\right) \tag{23}$$

where I_0 is the zero order modified Bessel function and the total current is $I_D = \pi r_e^2 J_D$. Equation (23) was integrated to give a plot of J_r/J_D versus r/σ, with r_e/σ as a parameter and is given as Fig. 6 in Reference 6. It is reproduced here as Fig. 6. Since the only forces acting on electrons in the drift region are due to space charge, we may write the equation of motion as

$$\frac{d^2r}{dt^2} = \eta E_r \tag{24}$$

where E_r is the radial electrical field acting on an electron with radial coordinate r. Since the beam is long and narrow, all electric lines of force may be considered to leave the beam radially so that E_r is simply obtained from Gauss' law. Equation (24) therefore becomes

$$\begin{aligned} \frac{d^2r}{dt^2} = \frac{\eta}{2\pi\epsilon_0 r} \int_0^r 2\pi\rho\, dr = \frac{\eta}{2\pi\epsilon_0 r} \int_0^r \frac{J(r)}{\sqrt{2\eta V_a}} 2\pi r\, dr \\ = \frac{\sqrt{\eta/(2V_a)}}{2\pi\epsilon_0 r} \int_0^r J(r) 2\pi r\, dr \end{aligned} \tag{25}$$

From (23) we note that the fraction of the total current within any radius depends only on r_e/σ and r/σ:

$$\begin{aligned} \frac{I_r}{I_D} = \frac{\int_0^r J(r)2\pi r\, dr}{\int_0^\infty J(r)2\pi r\, dr} = 2\left(\frac{\sigma}{r_e}\right)^2 \int_0^{r/\sigma} e^{-(r^2/2\sigma^2)} \\ \times \left[\int_0^{r_e/\sigma} \frac{R}{\sigma} e^{-(r^2/2\sigma^2)} I_0\left(\frac{rR}{\sigma^2}\right) d\left(\frac{R}{\sigma}\right)\right] \frac{r}{\sigma} d\left(\frac{r}{\sigma}\right) \equiv F\left(\frac{r}{\sigma}, \frac{r_e}{\sigma}\right) \end{aligned} \tag{26}$$

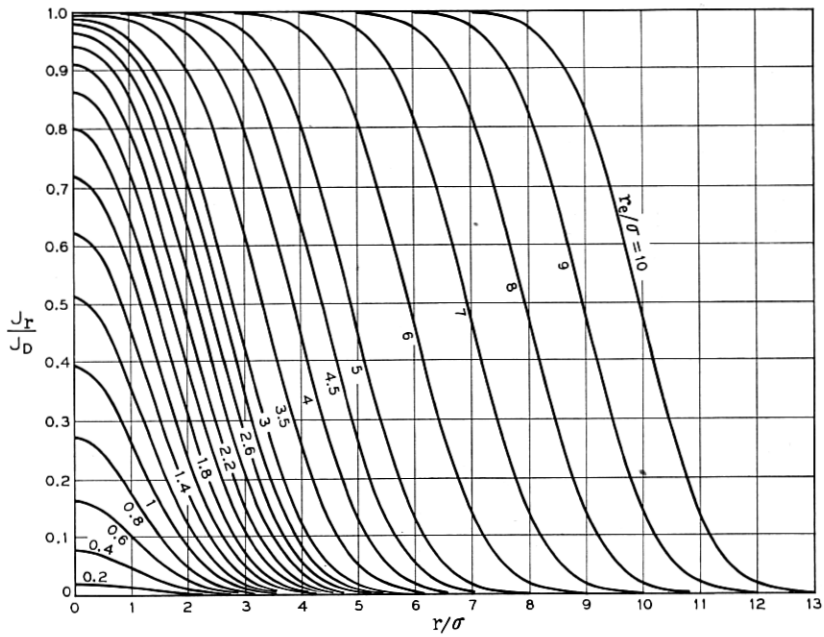

Fig. 6 — Curves showing the current density variation with radius in a beam which has been dispersed by thermal velocities. Here r_e is the nominal beam radius, r is the radius variable, and σ is the standard deviation defined in equation 17.

A family of curves with this ratio, F_r, as parameter has been reproduced from the Hines-Cutler paper and appears here as Fig. 7. Using this notation, (25) becomes

$$\frac{d^2r}{dt^2} = \frac{\sqrt{\eta/(2V_a)}}{2\pi\epsilon_0} I_D \frac{F_r}{r}$$

or

$$\frac{d^2r}{dz^2} = \frac{\eta}{2\pi\epsilon_0} \frac{I_D}{(2\eta V_a)^{3/2}} \frac{F_r}{r} \equiv K \frac{F_r}{r} \tag{27}$$

where we have made use of the dc electron drift velocity to make distance the independent variable instead of time, and have defined a quantity K which is proportional to gun perveance. We can now apply (27) to the motion of both the outer (edge) non-thermal electron and the σ-electron. From (26) we see that F_{r_e} and F_σ depend only on r_e/σ;

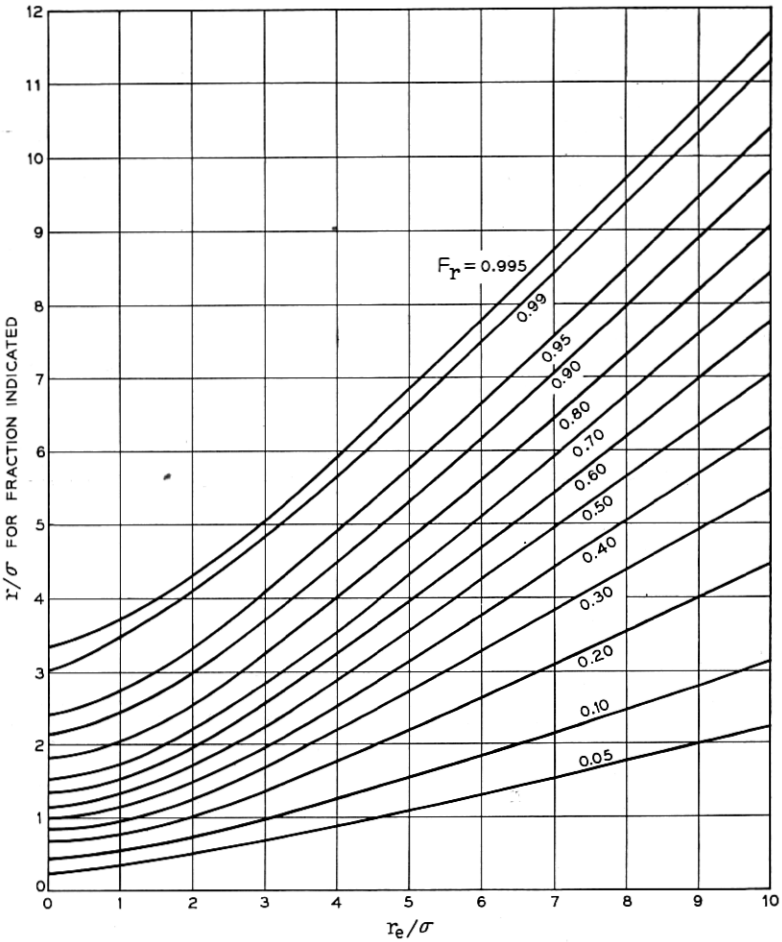

Fig. 7 — Curves showing the fraction, F_r, of the total beam current to be found within any given radius in a beam dispersed by thermal velocities as in Fig. 6.

consequently the continuous solution for r_e and r_σ $(= \sigma)$ as one moves axially along the drifting beam involves the simultaneous solution of two equations:

$$\frac{d^2 r_e}{dz^2} = KF_{r_e}/r_e$$
$$\frac{d^2 \sigma}{dz^2} = KF_\sigma/\sigma \tag{28}$$

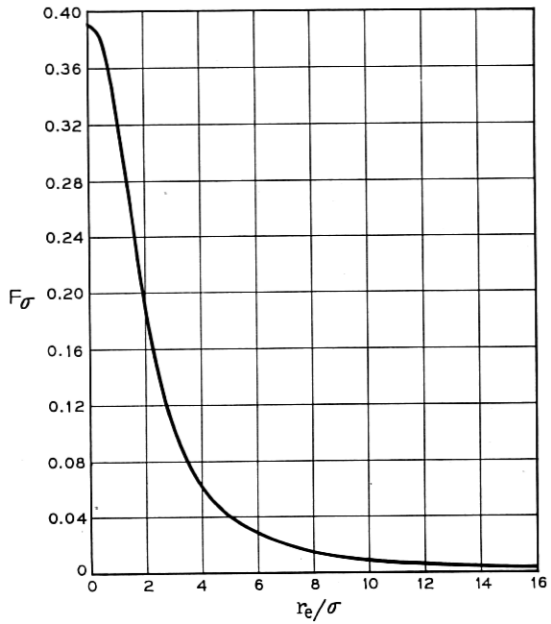

Fig. 8 — A curve showing the effect of a quantity related to the space charge force (in the drift region) on a thermal electron with standard deviation σ. (See equation 28.)

which are related by the mutual dependence of F_{r_e} and F_σ on r_e/σ. F_σ and F_{r_e}/r_e are plotted in Figs. 8 and 9.

We may summarize the treatment of the drift region, then, as follows:

(a) The input values of r_e and r_{e-}' at the entrance to the anode lens are obtained from the Pierce gun parameters r_a and θ, while the value of σ and σ_-' at the lens entrance can be obtained as mentioned above by integrating (15) from the cathode, where $\mu_c = 0$ and $(d\mu/dt)_c = 1$, to the anode plane. (The minus subscripts on r' and σ' indicate that these slopes are being evaluated on the gun side of the lens; a plus subscript will be used to indicate evaluation on the drift region side of the lens.) The values of r_e and σ on leaving the lens will of course be their entrance values in the drift region, and the effect of the lens on r_e' and σ' is simply found in terms of the anode lens correction factor Γ by use of (20). The value of σ at the anode can be obtained from (17) if μ is known there. In this regard, (15) can be integrated once to give

$$d\mu = \frac{1}{r_c}\left(\frac{dr}{dt}\right)_c \frac{dt}{(r_e/r_c)^2} \tag{29}$$

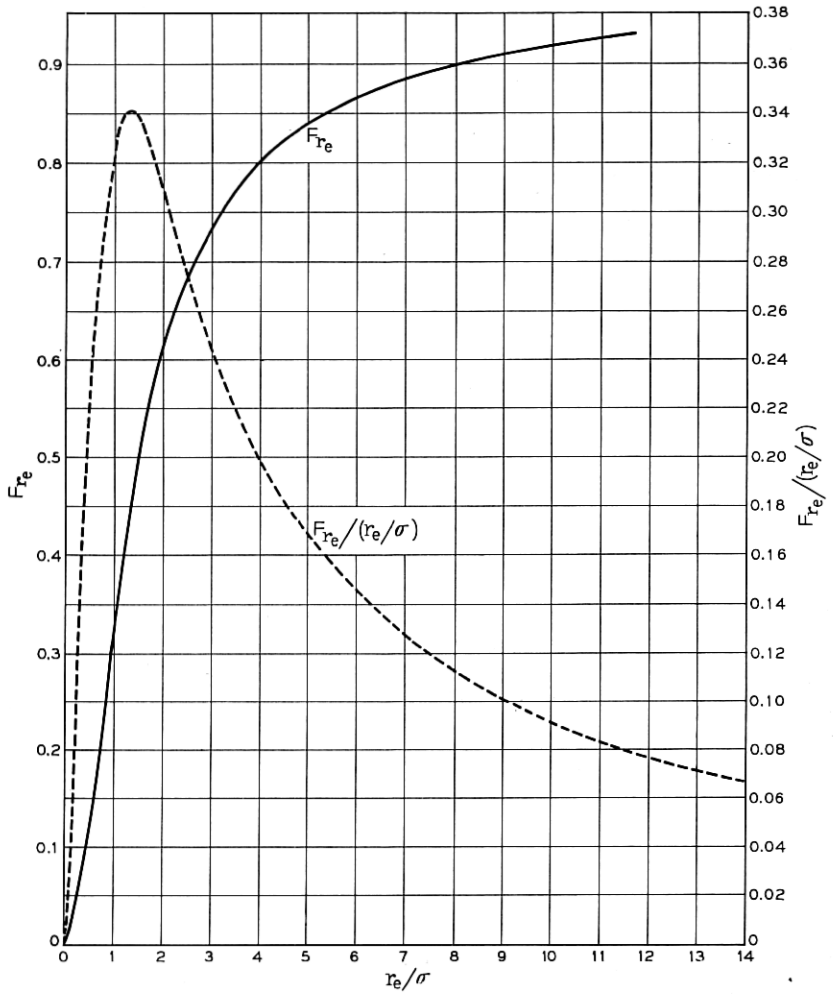

Fig. 9 — Showing quantities related to the effect of the space charge force in the drift region on the outermost non-thermal electron. (See equation 28.)

We can now substitute for transit time in terms of distance and Langmuir's well known potential function,[14] $-\alpha$. The value of this parameter, for the case of spherical cathode-anode geometry in which we are interested, depends only on the ratio $\bar{r}_c/\bar{r}$ which is equal to r_c/r_e. (Because of their frequent use in gun design, certain functions of $-\alpha$ are included here as Table I.) In terms of $-\alpha$, then, the potential in the gun region

TABLE I — TABLE OF FUNCTIONS OF $-\alpha$ OFTEN USED IN ELECTRON GUN DESIGN

$\bar{r}_c/\bar{r}$	$(-\alpha)^2$	$(-\alpha)^{4/3}$	$(-\alpha)^{2/3}$	$\int_1^{\bar{r}_c/\bar{r}} \frac{d\left(\frac{\bar{r}_c}{\bar{r}}\right)}{(-\alpha)^{2/3}}$	$\frac{d(-\alpha)^{4/3}}{d(\bar{r}_c/\bar{r})}$
1.0	0.0000	0.0000	0.0000	0.0000	
1.025	0.0006	0.0074			
1.05	0.0024	0.0179	0.134		
1.075	0.0052	0.0306	0.173		
1.10	0.0096	0.0452	0.212	1.392	0.590
1.15	0.0213	0.0768	0.277		
1.20	0.0372	0.1114	0.334	1.767	0.716
1.25	0.0571	0.1483	0.385		
1.30	0.0809	0.1870	0.432	2.031	0.790
1.35	0.1084	0.2273	0.476		
1.40	0.1396	0.2691	0.519	2.243	0.874
1.45	0.1740	0.3117	0.558		
1.50	0.2118	0.3553	0.596	2.423	0.886
1.60	0.2968	0.4450	0.667	2.583	0.915
1.70	0.394	0.5374	0.733	2.725	0.939
1.80	0.502	0.6316	0.795	2.855	0.954
1.90	0.621	0.7279	0.853	2.975	0.970
2.00	0.750	0.8255	0.908	3.087	0.982
2.10	0.888	0.9239	0.961	3.192	0.993
2.20	1.036	1.024	1.012	3.292	1.003
2.30	1.193	1.125	1.061	3.388	1.012
2.40	1.358	1.226	1.107	3.481	1.020
2.50	1.531	1.328	1.152	3.570	1.028
2.60	1.712	1.431	1.196	3.655	1.034
2.70	1.901	1.535	1.239	3.738	1.039
2.80	2.098	1.639	1.280	3.817	1.044
2.90	2.302	1.743	1.320	3.894	1.048
3.00	2.512	1.848	1.359	3.968	1.052
3.1	2.729	1.953	1.397	4.040	1.056
3.2	2.954	2.059	1.435	4.111	1.059
3.3	3.185	2.164	1.471	4.180	1.062
3.4	3.421	2.270	1.507	4.247	1.064
3.5	3.664	2.376	1.541	4.315	1.066
3.6	3.913	2.483	1.576	4.377	1.068
3.7	4.168	2.590	1.609	4.441	1.070
3.8	4.429	2.697	1.642	4.501	1.072
3.9	4.696	2.804	1.674	4.563	1.074
4.0	4.968	2.912	1.706	4.621	1.076

may be written

$$V = V_a(-\alpha)^{4/3}/(-\alpha_a)^{4/3} \tag{30}$$

$$dt = -\frac{d\bar{r}}{\sqrt{2\eta V}} = -\frac{d\bar{r}}{\sqrt{2\eta V_a}}\frac{(-\alpha_a)^{2/3}}{(-\alpha)^{2/3}} \tag{31}$$

so that upon substitution from (29) and (31), (17) becomes

$$\sigma = r_e\sqrt{\frac{T}{V_a}}\sqrt{\frac{k}{2e}}\frac{\bar{r}_c}{r_c}(-\alpha_a)^{2/3}\int_1^{\bar{r}_c/\bar{r}}(-\alpha)^{-2/3}\,d\left(\frac{\bar{r}_c}{\bar{r}}\right) \tag{32}$$

Fig. 5, which has been referred to above, shows

$$\frac{\sigma_a}{\bar{r}_c}\sqrt{\frac{2eV_a}{kT}}$$

as a function of $(\bar{r}_c/\bar{r}_a)$ as obtained from (32), and allows σ_a to be determined easily. Using (20), the value of r_{e+}' is given by

$$r_{e+}' = -\frac{r_{ea}}{F} + r_{e-}' = -\frac{r_{ea}}{F} - \theta_e = -\frac{\Gamma r_{ea}}{F_D} - \theta_e = \theta_e\left(-\frac{\Gamma\bar{r}_a}{F_D} - 1\right) \tag{33}$$

where θ_e is the half-angle of the cathode (and hence the initial angle which the path of a non-thermal edge electron makes with the axis). We may write for $1/F_D$

$$-\frac{1}{F_D} = \frac{V'}{4V} = \frac{\bar{r}_c}{4(-\alpha_a)^{4/3}\bar{r}_a^2}\left(\frac{d(-\alpha)^{4/3}}{d(\bar{r}_c/\bar{r})}\right)_a \tag{34}$$

In Fig. 10 we plot $-\bar{r}_a/F_D$ as a function of $\bar{r}_c/\bar{r}_a$ for easy evaluation of r_{e+}' in (33). Taking the first derivative of (32) with respect to z, we obtain an expression for σ_-'. Using this in conjunction with (20) and (34) we find

$$\sigma_+' = \sqrt{\frac{T}{V_a}}(\Gamma C_1 + C_2) \tag{35}$$

where

$$C_1 = \sqrt{\frac{k}{2e}}\frac{\bar{r}_c/\bar{r}_a}{4(-\alpha)^{2/3}}\left(\frac{d(-\alpha)^{4/3}}{d(\bar{r}_c/\bar{r})}\right)_a\int_1^{\bar{r}_c/\bar{r}_a}\frac{d(\bar{r}_c/\bar{r})}{(-\alpha)^{2/3}}$$

and

$$C_2 = \sqrt{\frac{k}{2e}}\left[\frac{\bar{r}_c}{\bar{r}_a} - (-\alpha_a)^{2/3}\int_1^{\bar{r}_c/\bar{r}_a}\frac{d(\bar{r}_c/\bar{r})}{(-\alpha)^{2/3}}\right]$$

C_1 and C_2 are plotted as functions of $\bar{r}_c/\bar{r}_a$ in Fig. 11.

(b) After choosing a specific value for Γ and evaluating $K = \eta I_D/$

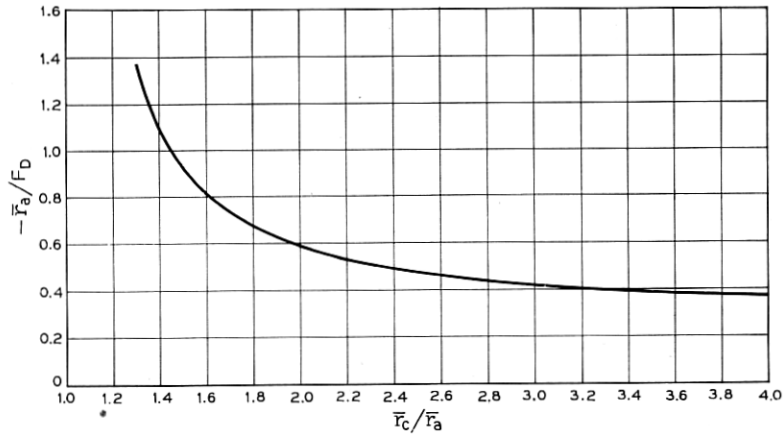

Fig. 10 — Curve used in finding r_{e+}', the direction of a nonthermal edge electron as it enters the drift region. (See equation 33.)

$(2\pi\epsilon_0(2\eta V_a)^{3/2})$, (28) is integrated numerically using the BTL analog computer to obtain σ and r_e as functions of axial distance along the beam.

(c) Knowing σ and r_e, other beam parameters such as current distribution and the radius of the circle which would encompass a given percentage of the total current can be found from Figs. 6 and 7.

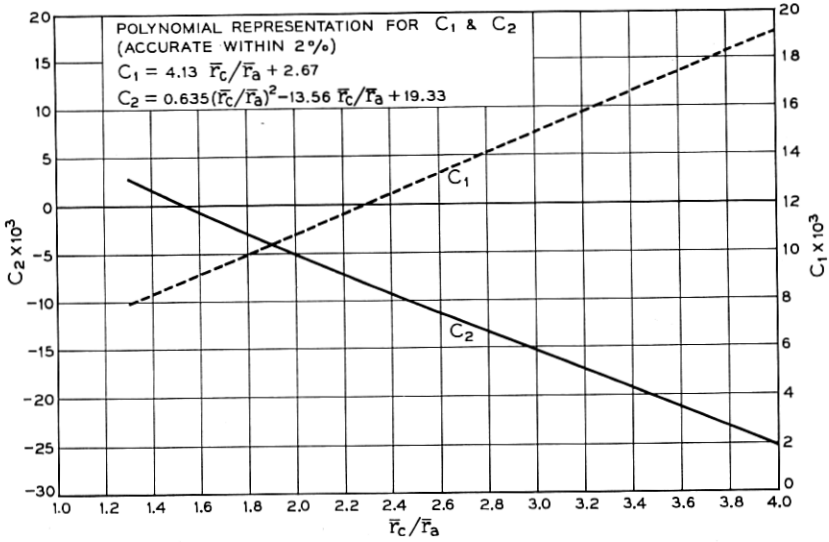

Fig. 11 — Curves used in evaluating σ_+', the slope of the trajectory of a thermal electron with standard deviation σ as it enters the drift region. (See equation 35.)

5. NUMERICAL DATA FOR ELECTRON GUN AND BEAM DESIGN

A. Choice of Variables

Except for a scaling parameter, the electrical characteristics of an ideal Pierce electron gun are completely determined when three parameters are specified, e.g., $\bar{r}_c/\bar{r}_a$, perveance, and V_a/T. Also, for the simplest case Γ is equal to 1 so that (since K depends only on gun perveance) in this case no additional parameter is needed. This implies that normalized values of r_e', σ, σ', and K at the drift side of the anode lens are not independent. If, however, the value of Γ at the anode lens is taken as an additional variable, four parameters plus simple scaling are required before complete predictions of beam characteristics can be made. In assembling analog computer data which would adequately cover values of $\bar{r}_c/\bar{r}_a$, perveance, and V_a/T which are likely to be of interest to us in designing future guns, we chose to present the major part of our data with Γ fixed at 1.1. This has seemed to be a rather typical value for Γ, and by choosing a specific value we decrease the total number of significant variables from 4 to 3. (The effect of variations in Γ on the minimum radius which contains 95 per cent of the beam is, however, included in Fig. 16 for particular values of V_a/T and perveance.) Although the boundary conditions for our mathematical description of the beam in a drift space are simplest when expressed in terms of r_e, r_e', σ and σ', we have attempted to make the results more usable by expressing all derived parameters in terms of $\bar{r}_c/\bar{r}_a$, $\sqrt{V_a/T}$, and the perveance, P.

B. Tabular Data

The rather extensive data obtained from the analog computer for the $\Gamma = 1.1$ case and for practical ranges in perveance, V_a/T, and $\bar{r}_c/\bar{r}_a$ are summarized in Tables IIA to E where the parameters r_e and σ which specify the beam cross section are given as functions of axial distance from the anode plane. Some feeling for the decrease in accuracy to be expected as the distance from the anode plane increases can be obtained by reference to Section 6B where experiment and theory are compared over a range of this axial distance parameter.

C. Graphical Data, Including Design Charts and Beam Profiles

In typical cases, the designer of Pierce electron guns is much more concerned with the beam radius at the axial position where it is smallest (and in the axial position of this minimum) than he is in the general

spreading of the beam with distance. This is true because, in microwave beam tubes, the beam from a magnetically shielded Pierce gun normally enters a strong axial magnetic field near a point where the radius is a minimum, so that magnetic focusing forces largely determine the beam's subsequent behavior. The analog computer data has therefore been reprocessed to stress the dependence of the beam's minimum diameter and the corresponding axial position of the minimum on the basic design parameters $\bar{r}_c/\bar{r}_a$, perveance, and $\sqrt{V_a/T}$. As a first step in this direction, the radius, r_{95}, of a circle which includes 95 per cent of the beam current is obtained as a function of axial position along the beam. Such data are shown graphically in Fig. 12. Finally, the curves of Fig. 12 are used in conjunction with the tabular data to obtain the "Design Curves" of Fig. 13 where all of the pertinent information relating to the beam at its minimum diameter is presented.

D. Example of Gun Design Using Design Charts

Assume that we desire an electron gun with the following properties: anode voltage $V_A = 1{,}080$ volts, cathode current $I_D = 7.1$ ma, and minimum beam diameter $2(r_{95})_{\min} = 0.015$ inches. Let us further assume a cathode temperature $T = 1080°$ Kelvin, an available cathode emission density of 190 ma per square cm, and an anode lens correction factor of $\Gamma = 1.1$. From these data we find $\sqrt{V_a/T} = 1.0$, perveance $P = 0.2 \times 10^{-6}$ amps/(volts)$^{3/2}$ and $(r_{95})_{\min}/r_c = 0.174$. Reference to the design chart, Fig. 13, now gives us the proper value for $\bar{r}_c/\bar{r}_a$: using the upper set of curves in the column for $\sqrt{V_a/T} = 1.0$ we note the point of intersection between the horizontal line for $(r_{95})_{\min}/r_c = 0.174$ and the perveance line $P = 0.2$, and read the value of $\bar{r}_c/\bar{r}_a$ $(= 2.8)$ as the corresponding abscissa. The convergence angle of the gun, θ_e, is now simply determined from the equation[15]

$$\theta_e = \cos^{-1}\left(1 - \frac{(-\alpha_a)^2 P}{14.67} \times 10^6\right) \tag{37}$$

(θ_e is found to be 13.7° in this example) and the potential distribution in the region of the cathode can be obtained from (30).

When this point has been reached, the gun design is complete except for the shapes of the beam forming electrode and the anode, which are determined with the aid of an electrolytic tank in the usual way.[16] The radius of the anode hole which will give a specified transmission can be found by obtaining $(r_e/\sigma)_a$ through the use of Fig. 5, and then choosing the anode radius from Fig. 7. In practical cases where $(r_e/\sigma)_a > 3.0$,

TABLE IIA — SUMMARY OF ANALOG COMPUTER DATA FOR AN ANODE LENS CORRECTION OF $\Gamma = 1.1$ FOR PERVEANCE $= 0.05 \times 10^{-6}$ AMPS/(VOLTS)$^{3/2}$

$\bar{r}_e/\bar{r}_a = 1.515$			2.0			2.5			3.0			3.5			4.0			
$\frac{z}{r_a}$	$\frac{r_e}{\sigma}$	$\frac{\sigma}{r_a}$	$\frac{z}{r_a}$	$\frac{r_e}{\sigma}$	$\frac{\sigma}{r_a}$	$\frac{z}{r_a}$	$\frac{r_e}{\sigma}$	$\frac{\sigma}{r_a}$	$\frac{z}{r_a}$	$\frac{r_e}{\sigma}$	$\frac{\sigma}{r_a}$	$\frac{z}{r_a}$	$\frac{r_e}{\sigma}$	$\frac{\sigma}{r_a}$	$\frac{z}{r_a}$	$\frac{r_e}{\sigma}$	$\frac{\sigma}{r_a}$	
0	2.02	0.495	0	1.95	0.513	0	1.90	0.527	0	1.85	0.540	0	1.81	0.552	0	1.75	0.565	
2	1.90	0.535	1	1.86	0.528	2	1.68	0.545	2	1.60	0.545	2	1.5	0.55	2	1.44	0.549	
4	1.76	0.579	2	1.78	0.541	4	1.45	0.560	4	1.35	0.560	4	1.19	0.548	4	1.07	0.531	
6	1.65	0.620	3	1.67	0.556	6	1.24	0.580	6	1.08	0.555	6	0.86	0.548	6	0.69	0.519	
8	1.55	0.669	4	1.60	0.570	8	1.04	0.600	8	0.82	0.565	8	0.53	0.548	8	0.27	0.505	
			6	1.44	0.601	10	0.86	0.621	10	0.58	0.575	10	0.20	0.552	10	−0.12	0.498	$\sqrt{V_a/T} = 0.5$
			8	1.30		12	0.69	0.645	12	0.35	0.589	12	−0.10	0.558	12	−0.56	0.490	
			10	1.18	0.669	14	0.52	0.670	14	0.13	0.602	14	−0.40	0.563	14	−1.01	0.485	
			12	1.05	0.701	16	0.38	0.700	16	−0.10	0.619	16	−0.70	0.575	16	−1.48	0.482	
						18	0.25	0.725	20	−0.47	0.657	18	−1.0	0.585	18	−1.92	0.482	
						20	0.12	0.760	24	−0.81	0.702	20	−1.25	0.60	20	−2.38	0.485	
						22	0	0.790	26	−0.96	0.729	22	−1.53	0.615				
0	4.03	0.248	0	3.91	0.256	0	3.78	0.264	0	3.70	0.270	0	3.62	0.276	0	3.56	0.281	
2	3.74	0.267	2	3.55	0.270	2	3.32	0.273	2	3.15	0.273	2	3.0	0.273	2	2.85	0.272	
4	3.48	0.288	4	3.20	0.285	4	2.87	0.281	4	2.62	0.277	4	2.35	0.273	4	2.11	0.265	
6	3.25	0.310	6	2.89	0.302	6	2.46	0.292	6	2.1	0.282	6	1.71	0.274	6	1.32	0.260	
8	3.06	0.332	8	2.61	0.318	8	2.08	0.308	8	1.6	0.289	8	1.06	0.280	8	0.54	0.259	
10	2.88	0.358	10	2.35	0.338	10	1.71	0.318	10	1.1	0.299	10	0.45	0.286	9	0.15	0.260	
12	2.73	0.382	12	2.11	0.358	12	1.38	0.334	12	0.67	0.311	11	0.15	0.292	10	−0.25	0.262	
14	2.59	0.408	14	1.90	0.379	13	1.23	0.344	13	0.46	0.32	12	−0.12	0.299	12	−1.0	0.27	$\sqrt{V_a/T} = 1.0$
16	2.47	0.435	16	1.71	0.402	14	1.09	0.352	14	0.25	0.329	14	−0.63	0.314	14	−1.71	0.282	
20	2.26	0.492	20	1.40	0.456	16	0.83	0.374	16	−0.10	0.349	16	−1.1	0.332	16	−2.36	0.297	
24	2.09	0.553	24	1.14	0.516	20	0.38	0.426	18	−0.42	0.372	20	−1.86	0.380	18	−2.94	0.312	
26	2.02	0.588	28	0.95	0.582	24	0.06	0.489	20	−0.68	0.40	24	−2.43	0.433	20	−3.44	0.33	
						28	−0.20	0.561	24	−1.13	0.463	28	−2.87	0.492	24	−4.31	0.368	
									28	−1.47	0.535							

0	8.05	0.124	0	7.81	0.128	0	7.57	0.132	0	7.40	0.135	0	7.25	0.138	0	7.08	0.141	
4	6.94	0.145	4	6.4	0.142	4	5.77	0.140	4	5.3	0.138	4	4.7	0.135	4	4.2	0.132	
8	6.12	0.166	8	5.2	0.159	8	4.19	0.151	8	3.23	0.143	8	2.1	0.140	8	1.05	0.130	
12	5.5	0.191	12	4.25	0.180	12	2.81	0.168	12	1.40	0.158	10	0.9	0.148	9	0.30	0.135	
16	5.0	0.218	16	3.5	0.201	14	2.37	0.180	13	1.00	0.165	11	0.3	0.154	10	−0.32	0.140	
20	4.61	0.246	20	2.9	0.230	16	1.72	0.192	14	0.63	0.172	12	−0.1	0.161	11	−1.00	0.147	
24	4.30	0.276	24	2.4	0.265	18	1.29	0.210	15	0.30	0.182	14	−0.95	0.182	12	−1.60	0.155	$\sqrt{V_a/T} = 2.0$
28	4.02	0.310	28	2.0	0.305	20	0.90	0.232	16	0.03	0.193	16	−1.60	0.210	16	−3.25	0.201	
32	3.82	0.345	32	1.7	0.358	24	0.38	0.290	20	−0.79	0.255	20	−2.42	0.275	20	−4.25	0.255	
36	3.67	0.384	36	1.5	0.417	28	0.05	0.364	24	−1.28	0.331	24	−2.90	0.349	24	−4.85	0.31	
40	3.51	0.425	40	1.31	0.484	32	−0.18	0.453	28	−1.57	0.422	28	−3.25	0.425	28	−5.30	0.37	
			44	1.2	0.560	36	−0.31	0.552	32	−1.73	0.52	32	−3.45	0.504				
			48	1.1	0.640				36	−1.87	0.622							

Table IIB — Summary of Analog Computer Data for Anode Lens Correction of $\Gamma = 1.1$ for Perveance $= 0.1 \times 10^{-6}$ amps/(volts)$^{3/2}$

$\bar{r}_c/\bar{r}_a = 1.515$			2.0			2.5			3.0			3.5			4.0			
$\frac{z}{r_a}$	$\frac{r_e}{\sigma}$	$\frac{\sigma}{r_a}$	$\frac{z}{r_a}$	$\frac{r_e}{\sigma}$	$\frac{\sigma}{r_a}$	$\frac{z}{r_a}$	$\frac{r_e}{\sigma}$	$\frac{\sigma}{r_a}$	$\frac{z}{r_a}$	$\frac{r_e}{\sigma}$	$\frac{\sigma}{r_a}$	$\frac{z}{r_a}$	$\frac{r_e}{\sigma}$	$\frac{\sigma}{r_a}$	$\frac{z}{r_a}$	$\frac{r_e}{\sigma}$	$\frac{\sigma}{r_a}$	
0	2.85	0.350	0	2.75	0.363	0	2.69	0.372	0	2.60	0.382	0	2.56	0.390	0	2.52	0.397	
2	2.57	0.389	2	2.37	0.390	2	2.25	0.386	2	2.01	0.384	2	1.95	0.382	2	1.83	0.378	
4	2.32	0.431	4	2.04	0.421	4	1.82	0.405	4	1.56	0.391	4	1.30	0.382	4	1.05	0.365	
6	2.13	0.478	6	1.76	0.456	6	1.43	0.428	6	1.06	0.403	6	0.65	0.388	5	0.65	0.360	
8	1.95	0.525	8	1.52	0.492	8	1.07	0.452	8	0.60	0.420	7	0.35	0.392	6	0.24	0.358	
10	1.82	0.576	10	1.31	0.534	10	0.77	0.482	10	0.16	0.440	8	0.05	0.399	7	−0.15	0.357	
12	1.70	0.628	12	1.13	0.579	12	0.50	0.519	12	−0.18	0.467	9	−0.22	0.405	8	−0.56	0.357	$\sqrt{V_a/T} = 0.5$
14	1.60	0.683	14	0.97	0.625	14	0.26	0.557	14	−0.52	0.500	10	−0.51	0.415	10	−1.38	0.363	
			16	0.84	0.675	16	0.06	0.601	16	−0.82	0.537	11	−0.77	0.424	12	−2.16	0.372	
			18	0.73	0.730	18	−0.09	0.649	18	−1.07	0.575	12	−1.04	0.437	14	−2.90	0.385	
						20	−0.24	0.700	20	−1.29	0.620	14	−1.50	0.461	15	−3.23	0.392	
						22	−0.37	0.754	22	−1.48	0.668	16	−1.92	0.490	16	−3.57	0.400	
												18	−2.29	0.521				
												19	−2.46	0.537				

Table IIB (Continued)

$\bar{r}_c/\bar{r}_a = 1.515$			2.0			2.5			3.0			3.5			4.0			
$\frac{z}{r_a}$	$\frac{r_e}{\sigma}$	$\frac{\sigma}{r_a}$	$\frac{z}{r_a}$	$\frac{r_e}{\sigma}$	$\frac{\sigma}{r_a}$	$\frac{z}{r_a}$	$\frac{r_e}{\sigma}$	$\frac{\sigma}{r_a}$	$\frac{z}{r_a}$	$\frac{r_e}{\sigma}$	$\frac{\sigma}{r_a}$	$\frac{z}{r_a}$	$\frac{r_e}{\sigma}$	$\frac{\sigma}{r_a}$	$\frac{z}{r_a}$	$\frac{r_e}{\sigma}$	$\frac{\sigma}{r_a}$	
0	5.72	0.175	0	5.48	0.182	0	5.37	0.186	0	5.23	0.191	0	5.13	0.195	0	5.05	0.198	
1	5.39	0.183	2	4.75	0.195	2	4.49	0.191	2	4.16	0.192	2	3.90	0.190	2	3.65	0.185	
2	5.10	0.193	4	4.1	0.210	4	3.63	0.200	6	2.10	0.201	4	2.61	0.190	4	2.12	0.180	
4	4.62	0.214	5	3.83	0.219	6	2.86	0.212	8	1.17	0.215	6	1.36	0.196	5	1.34	0.180	
8	3.91	0.262	6	3.55	0.228	8	2.17	0.228	9	0.75	0.224	7	0.78	0.201	6	0.50	0.180	
12	3.41	0.314	7	3.3	0.237	10	1.55	0.248	10	0.38	0.239	8	0.22	0.210	7	−0.20	0.185	
16	3.06	0.374	8	3.09	0.248	11	1.28	0.259	12	−0.21	0.270	9	−0.27	0.220	8	−0.91	0.192	
20	2.79	0.441	10	2.66	0.270	12	1.04	0.273	14	−0.70	0.311	10	−0.72	0.234	10	−2.15	0.218	$\sqrt{V_a/T} = 1.0$
24	2.58	0.514	12	2.31	0.294	14	0.63	0.306	16	−1.06	0.360	12	−1.5	0.266	12	−3.10	0.245	
26	2.49	0.554	16	1.75	0.357	16	0.31	0.348	18	−1.33	0.412	14	−2.08	0.304	14	−3.88	0.275	
			20	1.36	0.435	20	−0.10	0.449	20	−1.54	0.471	16	−2.51	0.349	16	−4.46	0.306	
			24	1.09	0.529	24	−0.35	0.570	22	−1.70	0.531	18	−2.85	0.392	18	−4.95	0.340	
			28	0.90	0.638	28	−0.52	0.710	24	−1.83	0.599	20	−3.1	0.442				
			32	0.77	0.760													
0	11.35	0.088	0	11.0	0.091	0	10.75	0.093	0	10.40	0.096	0	10.2	0.098	0	10.10	0.099	
2	10.05	0.096	2	9.4	0.095	2	8.90	0.095	2	8.20	0.095	2	7.65	0.092	2	7.20	0.094	
4	9.15	0.106	4	8.1	0.103	4	7.20	0.101	4	6.20	0.100	4	5.12	0.091	4	4.20	0.092	
6	8.39	0.118	6	7.0	0.111	6	5.67	0.107	6	4.20	0.101	6	2.65	0.100	5	2.60	0.091	
8	7.75	0.130	8	6.08	0.120	8	4.33	0.115	8	2.40	0.110	7	1.45	0.103	6	1.00	0.083	
10	7.22	0.143	10	5.3	0.132	10	3.15	0.126	9	1.60	0.115	8	0.40	0.111	7	−0.28	0.100	
12	6.80	0.156	12	4.6	0.145	12	2.12	0.141	10	0.90	0.124	9	−0.39	0.124	8	−1.47	0.113	
16	6.15	0.186	14	4.03	0.160	13	1.72	0.151	11	0.32	0.138	10	−1.05	0.142	10	−3.05	0.149	$\sqrt{V_a/T} = 2.0$
20	5.65	0.218	16	3.55	0.176	14	1.37	0.164	12	−0.08	0.154	12	−1.98	0.186	12	−3.95	0.189	
24	5.25	0.254	18	3.15	0.194	16	0.80	0.197	14	−0.68	0.200	14	−2.5	0.237	14	−4.62	0.230	
28	4.95	0.293	20	2.80	0.216	20	0.20	0.295	16	−1.08	0.259	16	−2.85	0.292	16	−4.95	0.274	
32	4.75	0.336	24	2.25	0.270	24	−0.05	0.427	20	−1.43	0.393	18	−3.08	0.350	18	−5.22	0.317	
34	4.65	0.357	28	1.93	0.339	28	−0.18	0.580	24	−1.65	0.548	20	−3.2	0.408	20	−5.45	0.385	
			32	1.70	0.421	32	−0.21	0.751	28	−1.73	0.710	22	−3.33	0.467				
			36	1.50	0.305													

TABLE IIC — SUMMARY OF ANALOG COMPUTER DATA FOR AN ANODE LENS CORRECTION OF $\Gamma = 1.1$ FOR PERVEANCE $= 0.2 \times 10^{-6}$ AMPS/(VOLTS)$^{3/2}$

$\bar{r}_c/\bar{r}_a = 1.515$			1.97			2.54			3.15			3.46			4.0			
$\frac{z}{r_a}$	$\frac{r_e}{\sigma}$	$\frac{\sigma}{r_a}$	$\frac{z}{r_a}$	$\frac{r_e}{\sigma}$	$\frac{\sigma}{r_a}$	$\frac{z}{r_a}$	$\frac{r_e}{\sigma}$	$\frac{\sigma}{r_a}$	$\frac{z}{r_a}$	$\frac{r_e}{\sigma}$	$\frac{\sigma}{r_a}$	$\frac{z}{r_a}$	$\frac{r_e}{\sigma}$	$\frac{\sigma}{r_a}$	$\frac{z}{r_a}$	$\frac{r_e}{\sigma}$	$\frac{\sigma}{r_a}$	
0	4.05	0.247	0	3.9	0.258	0	3.75	0.266	0	3.63	0.276	0	3.55	0.282	0	3.48	0.287	$\sqrt{V_a/T} = 0.5$
2	3.55	0.290	2	3.2	0.290	2	2.85	0.282	2	2.52	0.278	2	2.37	0.282	2	2.05	0.270	
4	3.12	0.335	4	2.62	0.322	4	2.05	0.305	4	1.42	0.285	4	1.14	0.282	4	0.45	0.261	
6	2.77	0.380	6	2.15	0.360	6	1.35	0.331	6	0.45	0.308	5	0.55	0.285	4.5	0.05	0.265	
8	2.51	0.432	8	1.75	0.408	8	0.78	0.370	8	−0.38	0.341	6	0.00	0.296	5	−0.31	0.266	
10	2.30	0.490	10	1.45	0.459	10	0.34	0.420	10	−1.02	0.390	8	−1.00	0.325	6	−1.06	0.275	
12	2.12	0.550	12	1.21	0.520	12	0.00	0.480	12	−1.51	0.450	10	−1.78	0.370	8	−2.42	0.300	
14	1.98	0.614	14	1.01	0.580	14	−0.25	0.549	14	−1.88	0.515	12	−2.39	0.420	10	−3.52	0.330	
			16	0.87	0.655	16	−0.46	0.625	16	−2.15	0.588				12	−4.44	0.365	
			18	0.75	0.735	18	−0.61	0.710										
0	8.1	0.123	0	7.75	0.129	0	7.5	0.133	0	7.25	0.138	0	7.1	0.141	0	6.95	0.144	$\sqrt{V_a/T} = 1.0$
2	7.0	0.145	2	6.30	0.147	2	5.7	0.142	2	5.00	0.140	2	4.7	0.140	2	4.1	0.134	
4	6.15	0.166	4	5.20	0.163	4	4.1	0.153	4	2.85	0.145	4	2.25	0.140	4	0.95	0.135	
6	5.5	0.192	6	4.25	0.182	6	2.7	0.170	6	0.92	0.160	6	0.0	0.148	4.5	0.2	0.138	
8	5.0	0.216	8	3.5	0.205	8	1.59	0.195	7	0.12	0.178	8	−1.5	0.201	5	0.5	0.141	
10	4.6	0.244	10	2.95	0.234	10	0.75	0.237	8	−0.42	0.200	10	−2.35	0.264	6	1.72	0.160	
12	4.3	0.274	12	2.45	0.268	12	0.25	0.299	10	−1.27	0.261	12	−2.85	0.332	8	3.45	0.205	
14	4.02	0.306	14	2.10	0.301	14	−0.10	0.375	12	−1.76	0.339	14	−3.19	0.408	10	4.49	0.255	
16	3.8	0.34	16	1.80	0.358	16	−0.30	0.470	14	−2.08	0.423				12	5.15	0.310	
18	3.65	0.378	20	1.42	0.475	18	−0.45	0.570	16	−2.25	0.513							
20	3.5	0.42	24	1.20	0.625	20	−0.52	0.680	18	−2.40	0.610							
0	16.0	0.063	0	15.5	0.065	0	15.05	0.067	0	14.5	0.069	0	14.2	0.071	0	13.9	0.072	$\sqrt{V_a/T} = 2.0$
2	13.6	0.073	2	12.5	0.074	2	11.6	0.070	2	9.9	0.070	2	9.2	0.071	2	8.1	0.068	
4	12.1	0.084	4	10.3	0.080	4	8.3	0.075	4	5.7	0.072	4	4.4	0.071	4	1.9	0.068	
6	10.8	0.096	6	8.5	0.090	6	5.5	0.083	6	2.0	0.081	5	2.1	0.074	4.5	0.4	0.071	
8	9.8	0.110	8	7.1	0.101	8	3.4	0.095	7	0.5	0.094	6	0.2	0.085	5	−0.8	0.080	
10	9.1	0.124	10	6.0	0.115	10	1.8	0.119	8	−0.4	0.119	7	−1.0	0.108	6	−2.5	0.102	
12	8.5	0.139	12	5.1	0.131	12	0.8	0.165	10	−1.4	0.196	8	−1.8	0.140	8	−4.2	0.162	
14	8.05	0.156	14	4.45	0.151	14	0.3	0.235	12	−1.8	0.291	10	−2.58	0.220	10	−4.95	0.225	
16	7.65	0.174	16	3.9	0.175	16	0.1	0.330	14	−1.95	0.395	12	−2.9	0.305	12	−5.38	0.290	
18	7.35	0.193	20	3.2	0.236	18	−0.1	0.435	16	−2.05	0.505	14	−3.05	0.397	14	−5.60	0.360	
20	7.1	0.214	24	2.75	0.316	20	−0.1	0.558	18	−2.1	0.621	16	−3.15	0.492				
22	6.85	0.236	28	2.45	0.415	22	−0.15	0.685										
24	6.7	0.258	32	2.26	0.535	24	−0.2	0.820										

TABLE IID — SUMMARY OF ANALOG COMPUTER DATA FOR AN ANODE LENS CORRECTION OF $\Gamma = 1.1$ FOR PERVEANCE $= 0.4 \times 10^{-6}$ AMPS./(VOLTS)$^{3/2}$

$\bar{r}_c/\bar{r}_a = 1.515$			2.04			2.44			2.86			3.6			4.0			
$\frac{z}{r_a}$	$\frac{r_e}{\sigma}$	$\frac{\sigma}{r_a}$	$\frac{z}{r_a}$	$\frac{r_e}{\sigma}$	$\frac{\sigma}{r_a}$	$\frac{z}{r_a}$	$\frac{r_e}{\sigma}$	$\frac{\sigma}{r_a}$	$\frac{z}{r_a}$	$\frac{r_e}{\sigma}$	$\frac{\sigma}{r_a}$	$\frac{z}{r_a}$	$\frac{r_e}{\sigma}$	$\frac{\sigma}{r_a}$	$\frac{z}{r_a}$	$\frac{r_e}{\sigma}$	$\frac{\sigma}{r_a}$	
0	5.69	0.176	0	5.45	0.184	0	5.32	0.188	0	5.19	0.193	0	5	0.200	0	4.85	0.206	$\sqrt{V_a/T} = 0.5$
2	4.65	0.220	2	4.00	0.210	2	3.60	0.200	2	3.20	0.198	1	3.7	0.195	1	3.40	0.198	
4	3.92	0.268	4	2.95	0.242	4	2.29	0.230	4	1.50	0.220	2	2.35	0.192	2	1.86	0.192	
6	3.41	0.321	6	2.15	0.290	6	1.20	0.270	5	0.75	0.225	3	0.97	0.196	3	0.25	0.196	
8	3.09	0.382	8	1.60	0.350	8	0.49	0.341	6	0.18	0.270	4	−0.27	0.210	3.5	−0.45	0.201	
10	2.80	0.452	10	1.20	0.430	10	0.07	0.450	8	−0.65	0.360	5	−1.32	0.231	4	−1.15	0.210	
12	2.59	0.526	12	0.91	0.525	12	−0.18	0.570	10	−1.15	0.460	6	−2.15	0.265	5	−2.40	0.232	
			14	0.75	0.640	14	−0.32	0.705	12	−1.41	0.575	7	−2.78	0.300	6	−3.35	0.260	
			16	0.61	0.760	16	−0.45	0.860	14	−1.60	0.715	8	−3.26	0.340	7	−4.10	0.290	
												9	−3.65	0.380	8	−4.74	0.320	
0	11.4	0.088	0	10.9	0.092	0	10.7	0.094	0	10.3	0.097	0	10.0	0.100	0	9.75	0.103	$\sqrt{V_a/T} = 1.0$
2	9.3	0.108	2	8.1	0.106	2	7.2	0.100	2	6.6	0.099	1	7.5	0.098	1	6.8	0.097	
4	7.9	0.132	4	6.0	0.124	4	4.5	0.110	4	3.2	0.11	2	4.85	0.096	2	3.7	0.095	
6	6.9	0.156	6	4.5	0.147	6	2.4	0.135	6	0.5	0.15	3	2.1	0.099	3	0.50	0.098	
8	6.2	0.188	8	3.4	0.179	8	1.1	0.185	8	−0.6	0.25	3.5	0.80	0.104	4	−1.95	0.121	
10	5.7	0.220	10	2.6	0.220	10	0.42	0.275	10	−1.05	0.34	4	−0.32	0.115	5	−3.45	0.156	
12	5.3	0.256	12	2.08	0.280	12	0.18	0.40	12	−1.3	0.54	5	−1.9	0.15	6	−4.37	0.195	
14	5.0	0.293	14	1.7	0.352	14	0.00	0.54	14	−1.4	0.70	6	−2.8	0.195	7	−4.98	0.236	
16	4.8	0.336	16	1.5	0.445	16	−0.10	0.70				8	−3.7	0.292	8	−5.4	0.278	
18	4.6	0.380	20	1.25	0.675	18	−0.15	0.88				10	−4.1	0.398	9	−5.68	0.320	
0	22.8	0.044	0	21.8	0.046	0	21.3	0.047	0	20.7	0.048	0	20	0.05	0	19.5	0.052	$\sqrt{V_a/T} = 2.0$
2	18.5	0.052	2	17	0.050	2	14.7	0.050	2	12.5	0.050	1	14.6	0.049	1	13.4	0.050	
4	14.5	0.064	4	12.5	0.060	4	9.3	0.055	4	5.7	0.056	2	9.2	0.048	2	7.4	0.048	
6	13.7	0.078	6	9.5	0.070	6	5.2	0.070	6	1.0	0.082	3	3.8	0.049	3	1.3	0.049	
8	12.2	0.092	8	7.25	0.086	8	2.5	0.098	8	−0.50	0.174	3.5	1.3	0.052	4	−2.6	0.076	
10	11.3	0.108	10	5.6	0.110	10	1.2	0.16	10	−0.80	0.336	4	−0.60	0.062	5	−4.1	0.120	
12	10.6	0.126	12	4.6	0.140	12	0.75	0.265	12	−0.95	0.52	5	−2.45	0.106	6	−4.7	0.167	
14	10	0.146	14	3.9	0.175	14	0.60	0.405	14	−1.0	0.72	6	−3.15	0.160	7	−5.1	0.215	
16	9.7	0.168	16	3.5	0.222	16	0.49	0.57				7	−3.5	0.220	8	−5.35	0.265	
18	9.3	0.190	20	2.90	0.350	18	0.45	0.75				8	−3.65	0.281	9	−5.5	0.315	
			24	2.60	0.510	20	0.40	0.94				10	−3.82	0.410				

Table IIE — Summary of Analog Computer Data for an Anode Lens Correction of Γ = 1.1 for Perveance = 0.8×10^{-6} amps./(volts)$^{3/2}$

$\bar{r}_c/\bar{r}_a = 1.515$			2.0			2.5			3.0			3.5			4.0			
$\frac{z}{r_a}$	$\frac{r_e}{\sigma}$	$\frac{\sigma}{r_a}$	$\frac{z}{r_a}$	$\frac{r_e}{\sigma}$	$\frac{\sigma}{r_a}$	$\frac{z}{r_a}$	$\frac{r_e}{\sigma}$	$\frac{\sigma}{r_a}$	$\frac{z}{r_a}$	$\frac{r_e}{\sigma}$	$\frac{\sigma}{r_a}$	$\frac{z}{r_a}$	$\frac{r_e}{\sigma}$	$\frac{\sigma}{r_a}$	$\frac{z}{r_a}$	$\frac{r_e}{\sigma}$	$\frac{\sigma}{r_a}$	
0	8.00	0.125	0	7.7	0.130	0	7.42	0.135	0	7.15	0.140	0	6.85	0.146	0	6.62	0.151	$\sqrt{V_a/T} = 0.5$
2	6.1	0.165	2	5.0	0.160	2	4.05	0.153	2	2.85	0.150	1	4.3	0.140	1	3.64	0.142	
4	4.95	0.215	3	4.0	0.180	3	2.7	0.17	3	1.0	0.168	2	1.61	0.145	1.5	2.03	0.140	
6	4.21	0.275	4	3.3	0.202	4	1.55	0.196	3.5	0.20	0.184	2.5	0.40	0.155	2	0.4	0.142	
8	3.80	0.340	5	2.7	0.230	5	0.75	0.24	4	−0.30	0.205	3	−0.51	0.170	2.5	−0.95	0.153	
10	3.49	0.420	6	2.2	0.265	6	0.21	0.30	5	−1.05	0.265	4	−2.0	0.220	3	−2.15	0.17	
			8	1.6	0.360	8	−0.28	0.469	6	−1.52	0.345	5	−2.82	0.280	4	−3.85	0.214	
			10	1.2	0.490	10	−0.50	0.680	8	−2.0	0.530	6	−3.35	0.349	5	−4.95	0.260	
			12	1.0	0.645	12	−0.62	0.919	9	−2.15	0.625	7	−3.7	0.420	6	−5.71	0.310	
0	16.0	0.062	0	15.4	0.065	0	14.8	0.067	0	14.3	0.070	0	13.7	0.073	0	13.2	0.076	$\sqrt{V_a/T} = 1.0$
2	12.1	0.086	2	10	0.080	2	7.9	0.076	1	9.50	0.071	1	8.5	0.073	1	7.1	0.072	
4	9.85	0.110	4	6.6	0.100	4	3.1	0.10	2	5.6	0.075	2	3.4	0.074	1.5	4.0	0.070	
6	8.5	0.140	5	5.5	0.115	5	1.6	0.123	3	2.0	0.085	2.5	1.0	0.80	2	0.90	0.071	
8	7.65	0.175	6	4.5	0.130	6	0.70	0.170	3.5	0.60	0.100	3	−0.6	0.096	2.2	0.00	0.075	
10	7.1	0.215	7	3.9	0.154	8	0.08	0.340	4	−0.2	0.121	3.5	−1.71	0.125	2.5	−1.4	0.089	
12	6.7	0.259	8	3.3	0.180	10	−0.08	0.570	5	−1.1	0.200	4	−2.45	0.16	3.0	−3.1	0.112	
			10	2.6	0.250	12	−0.13	0.830	6	−1.5	0.295	5	−3.15	0.235	4.0	−4.7	0.170	
			12	2.15	0.345				7	−1.69	0.405	6	−3.5	0.315	5.0	−5.55	0.225	
			14	1.9	0.470				8	−1.79	0.518	7	−3.68	0.40	6.0	−6.0	0.289	
			16	1.7	0.610				9	−1.81	0.635							
0	32.1	0.031				0	29.7	0.034	0	28.5	0.035	0	27.5	0.0364	0	25.7	0.038	$\sqrt{V_a/T} = 2.0$
2	24.2	0.042				1	21.6	0.036	1	18.6	0.035	1	16.7	0.0364	1	14	0.036	
4	19.7	0.056				2	15.5	0.038	2	10.9	0.037	2	7.0	0.04	1.5	7.7	0.035	
6	17.2	0.071				3	10.5	0.042	3	3.9	0.042	2.5	2.4	0.056	2	1.6	0.035	
8	15.4	0.090				4	6.4	0.049	3.5	1.25	0.05	3	0.7	0.091	2.5	−2.1	0.050	
10	14.2	0.112				5	3.45	0.061	4	0.00	0.068	3.5	−2.1	0.131	3	−3.9	0.081	
12	13.4	0.134				6	1.7	0.089	5	−1	0.151	4	−2.6	0.221	4	−5.1	0.146	
14	12.8	0.160				7	0.9	0.145	6	−1.15	0.268	5	−3.0	0.316	5	−5.6	0.215	
						8	0.60	0.226	7	−1.25	0.395	6	−3.15	0.416	6	−5.85	0.285	
						9	0.50	0.330	8	−1.38	0.532	7	−3.25	0.520				
						10	0.48	0.447	9	−1.4	0.678	8	−3.3					
						12	0.40	0.71										

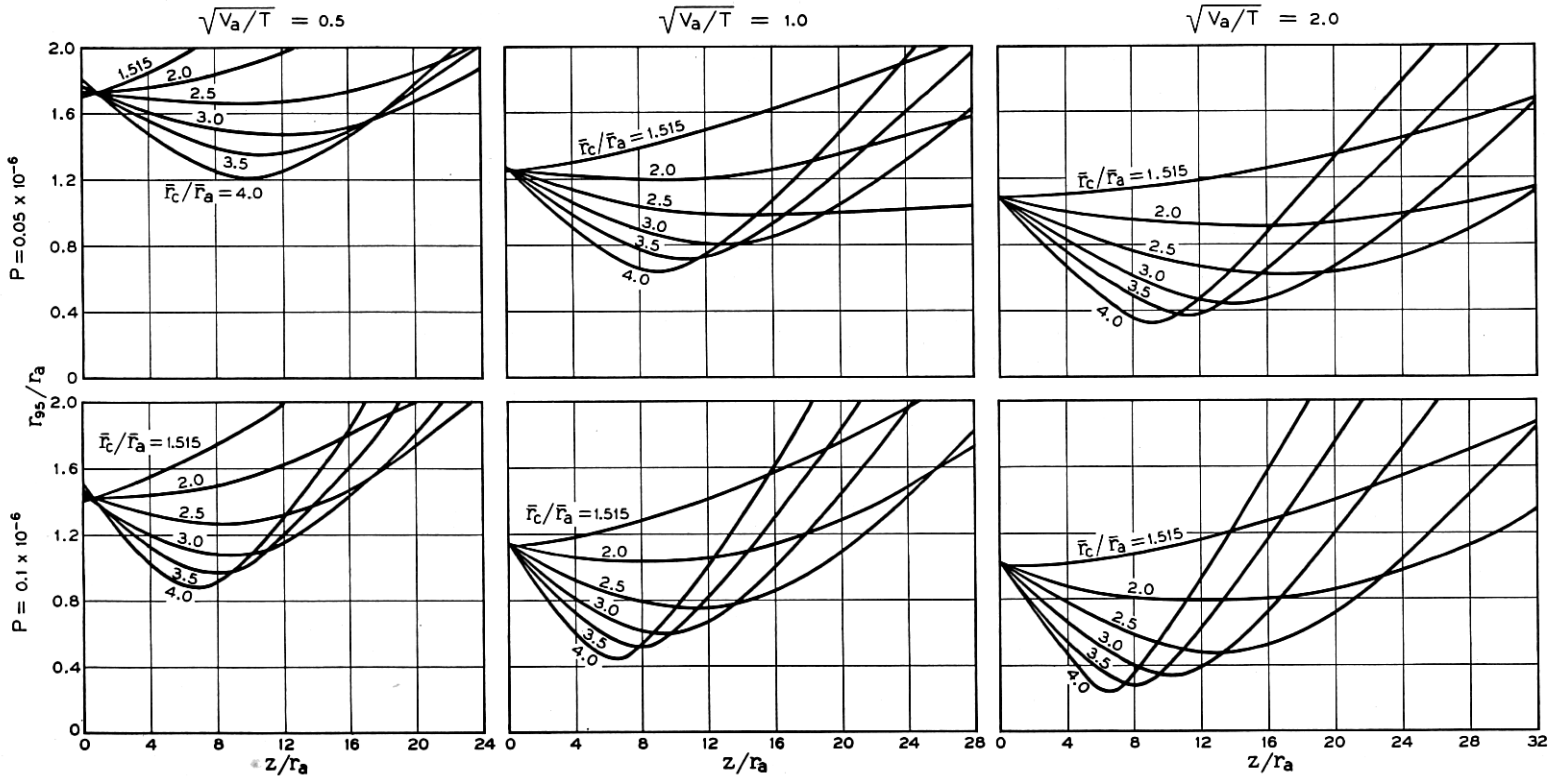

Fig. 12A — Curves showing normalized beam radius (95 per cent) versus distance from gun anode for variations in perveance (P), $\bar{r}_c/\bar{r}_a$ and $\sqrt{V_a/T}$.

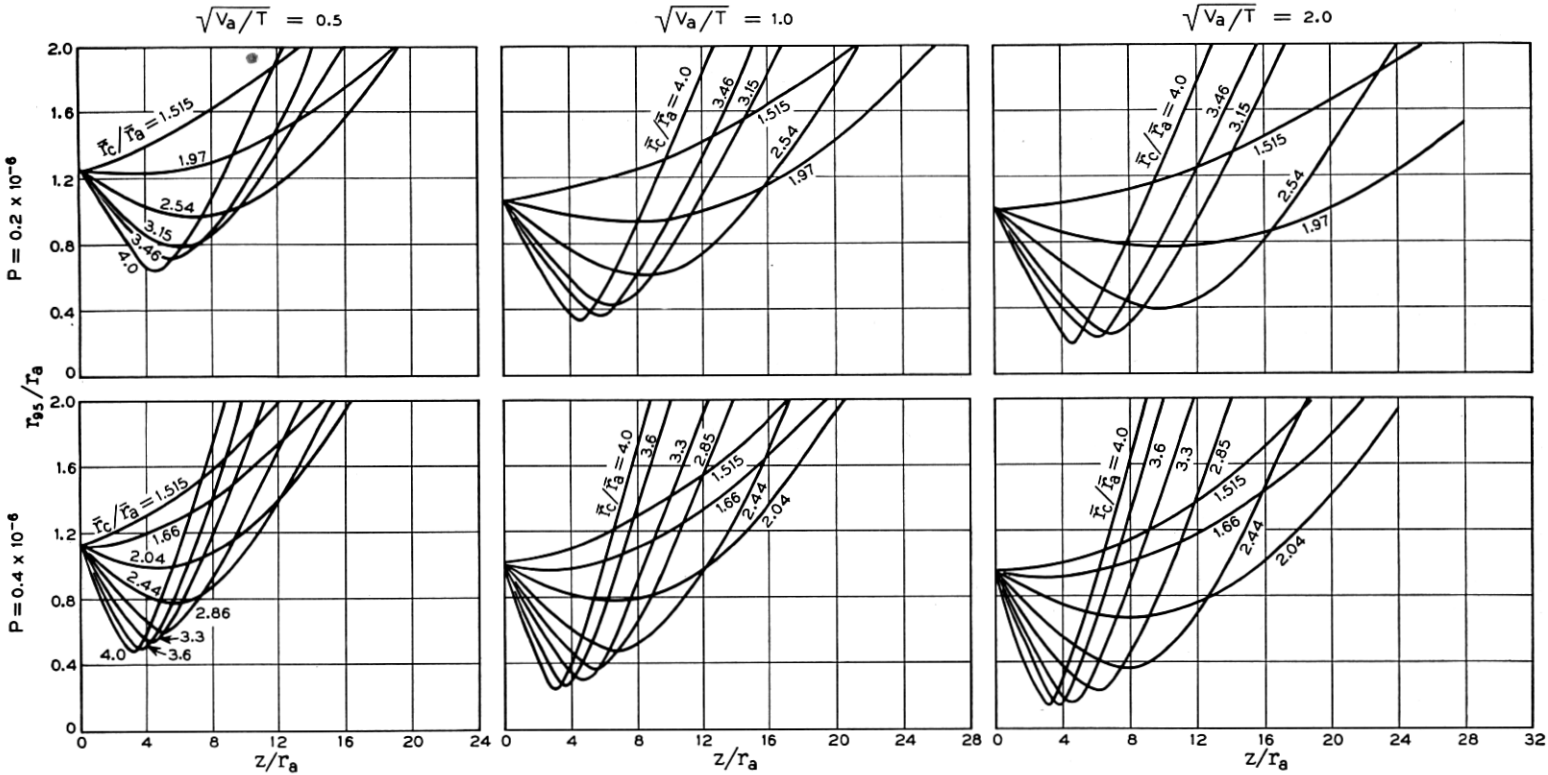

Fig. 12B — Curves showing normalized beam radius (95 per cent) versus distance from gun anode for variations in perveance (P), $\bar{r}_c/\bar{r}_a$ and $\sqrt{V_a/T}$.

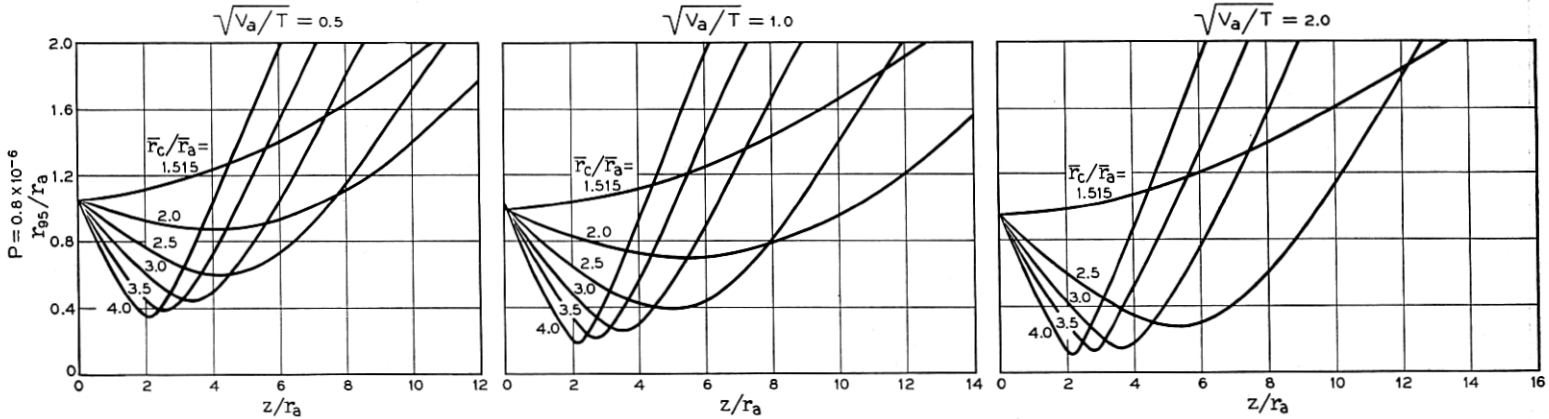

Fig. 12C — Curves showing normalized beam radius (95 per cent) versus distance from gun anode for variations in perveance (P), $\bar{r}_c/\bar{r}_a$ and $\sqrt{V_a/T}$.

we find less than 1 per cent anode interception if

$$\text{anode hole radius} = 0.93\, r_{ea} + 2\sigma_a \tag{38}$$

Additional information about the axial position of $(r_{95})_{\min}$ and the current density distribution in the corresponding transverse plane is contained in Fig. 13. The second set of curves in the $\sqrt{V_a/T} = 1$ column gives $z_{\min}/r_c = 2.42$ for this example, so that we would predict

$$z_{\min} \equiv \text{distance from anode to } (r_{95})_{\min} = 0.104''$$

The remaining 3rd and 4th sets of curves in the $\sqrt{V_a/T} = 1$ column allow us to find σ and r_e/σ at $z_{\min}$. In particular we obtain $\sigma = 0.0029''$ and $r_e/\sigma = 0.8$, and use Fig. 6 to give the current density distribution at $z_{\min}$.* Section VI contains experimental data which indicate a somewhat larger value for $z_{\min}$ than that obtained here. However the parameter of greatest importance, $(r_{95})_{\min}$, is predicted with embarrassing precision.

For those cases in which additional information is required about the beam shape at axial points other than $z_{\min}$, the curves of Fig. 12 or the data of Table II may be used.

6. COMPARISON OF THEORY WITH EXPERIMENT

In order to check the general suitability of the foregoing theory and the usefulness of the design charts obtained, several scaled-up versions of Pierce type electron guns, including the gun described in Section 5*D*, were assembled and placed in the double-aperture beam analyzer described in Reference 7.

A. Measurement of Current Densities in the Beam

Measurements of the current density distributions in several transverse planes near $z_{\min}$ were easily obtained with the aid of the beam analyzer. The resulting curve of relative current density versus radius at the experimental $z_{\min}$ is given in Fig. 14 for the gun of Section 5*D*. (This curve is further discussed in Part *C* below.) For this case, as well as for all others, special precautions were taken to see that the gun was functioning properly: In addition to careful measurement of the size and position of all gun parts, these included the determination that the distribution of transverse velocities at the center of the beam was smooth

* When $r_e/\sigma < 0.5$, the current density distribution depends almost entirely on σ, and, in only a minor way, on the ratio r_e/σ so that in such cases this ratio need not be accurately known.

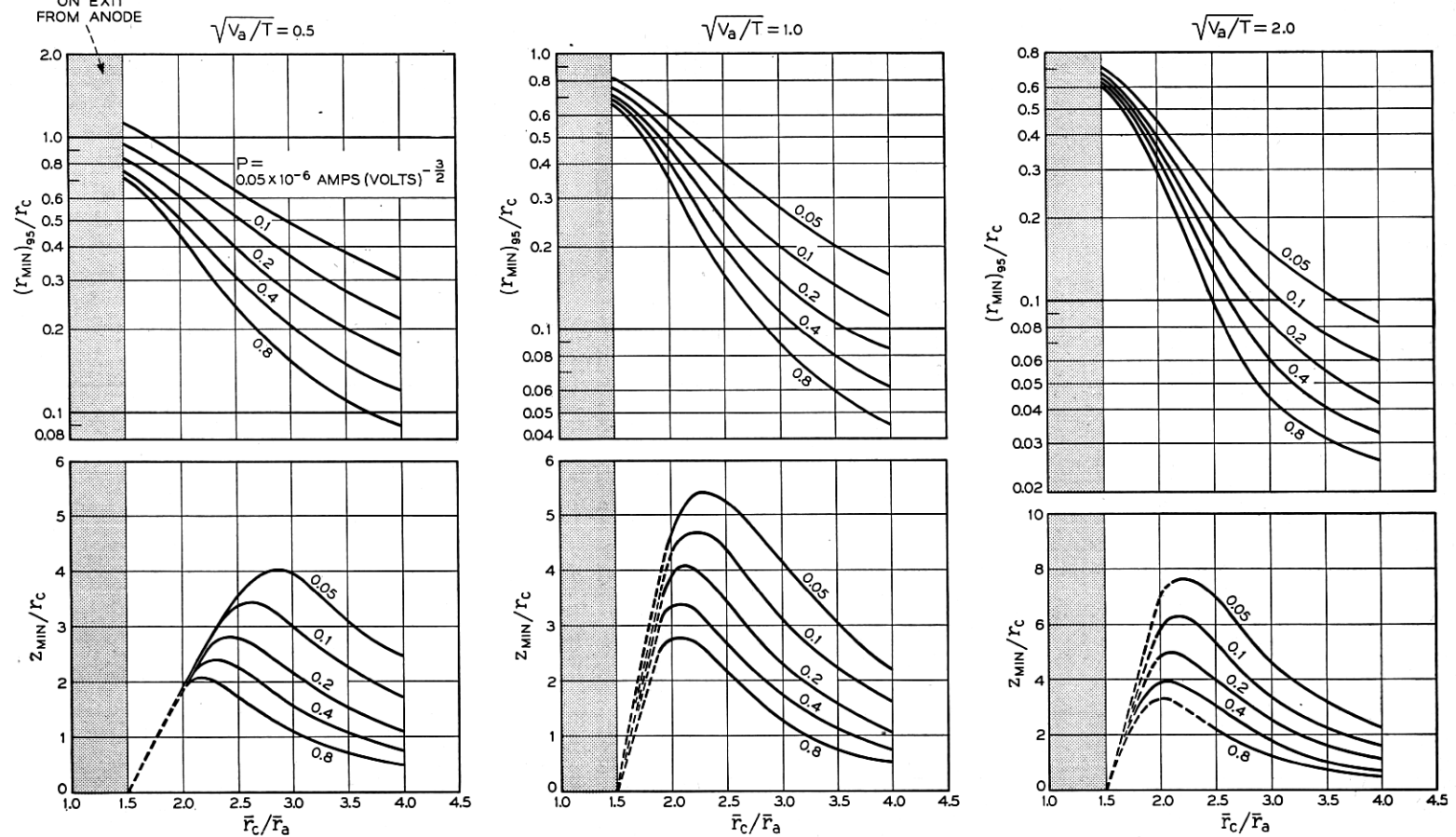

Fig. 13A — Design curves for Pierce-type electron guns considering transverse thermal velocities of electrons on emission from the cathode and an anode lens correction of $\Gamma = 1.1$. (for values of $r_e/\sigma < 0.5$, see footnote to Section 5*D*.)

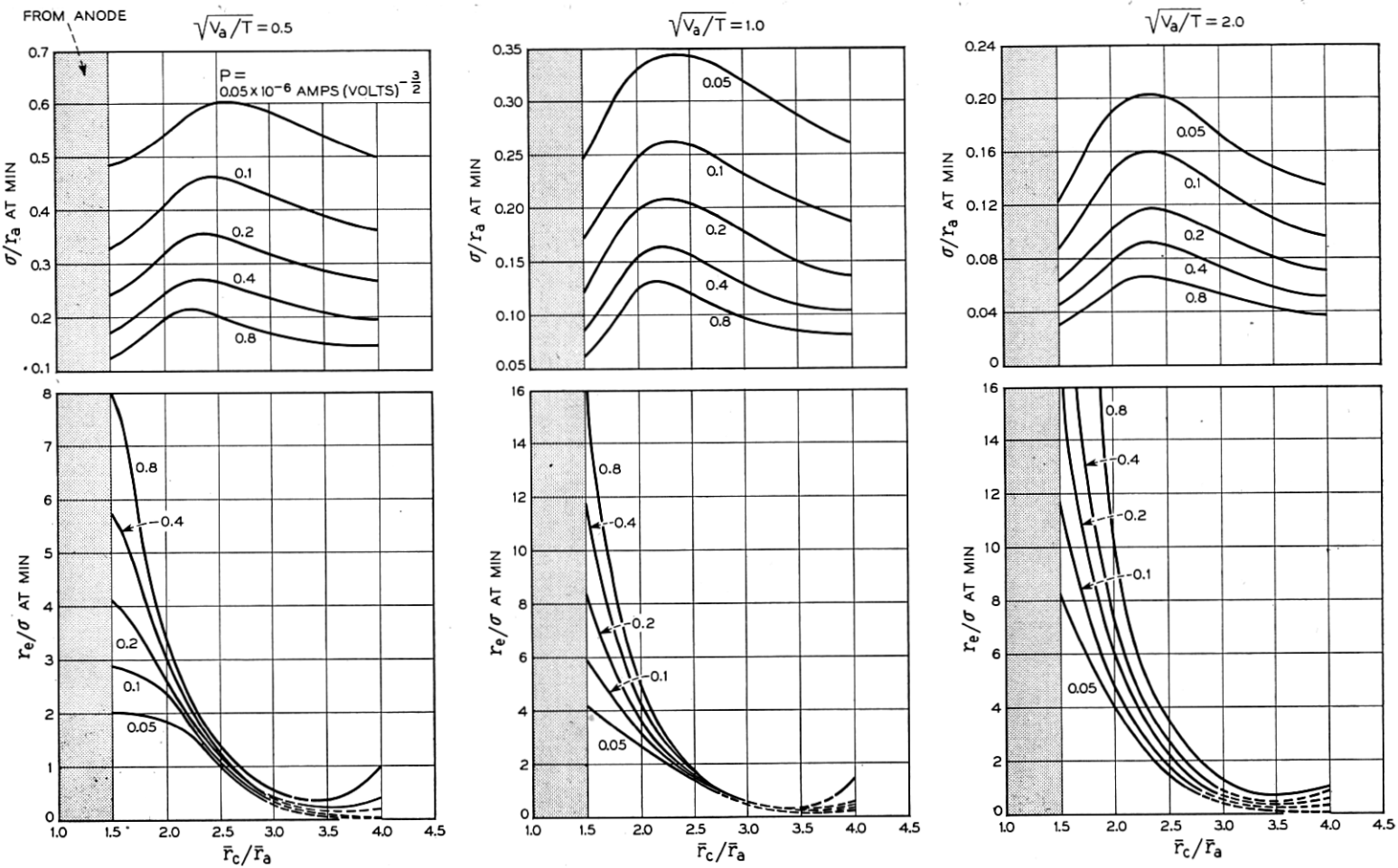
FROM ANODE
$\sqrt{V_a/T} = 0.5$
$\sqrt{V_a/T} = 1.0$
$\sqrt{V_a/T} = 2.0$
P = 0.05×10^{-6} AMPS (VOLTS)$^{-\frac{3}{2}}$
σ/r_a AT MIN
r_e/σ AT MIN
$\bar{r}_c/\bar{r}_a$
0.05
0.1
0.2
0.4
0.8

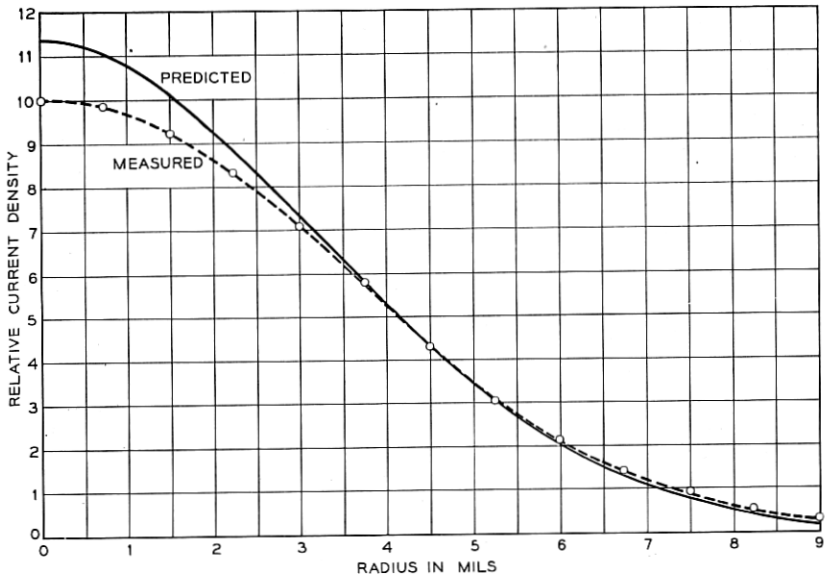

Fig. 14 — Current density distribution in a transverse plane located where the 95 per cent radius is a minimum. The predicted and measured curves are normalized to contain the same total current. (The corresponding prediction from the universal beam spread curve would show a step function with a constant relative current density of 64.2 for $r < 1.2$ mils and zero beyond.) The gun parameters are given in Section 5*D*.

and generally Gaussian in form, thereby indicating uniform cathode emission and proper boundary conditions at the edge of the beam near the cathode. The effect of positive ions on the beam shape was in every case reduced to negligible proportions, either by using special pulse techniques,[7] or by applying a small voltage gradient along the axis of the beam.

B. Comparison of the Experimentally Measured Spreading of a Beam with that Predicted Theoretically

From the experimentally obtained plots of current density versus radius at several axial positions along the beam, we have obtained at each position (by integrating to find the total current within any radius) a value for the radius, r_{95}, of that circle which encompasses 95 per cent of the beam. For brevity, we call the resulting plots of r_{95} versus axial distance, "beam profiles". The experimental profile for the gun described in Section 5*D* is shown as curve A in Fig. 15(a). Curve B shows the profile as predicted by the methods of this paper and obtained from Fig. 12. Curve C is the corresponding profile which one obtains by the Hines-Cutler method,[6] and Curve D represents r_{95} as obtained from the

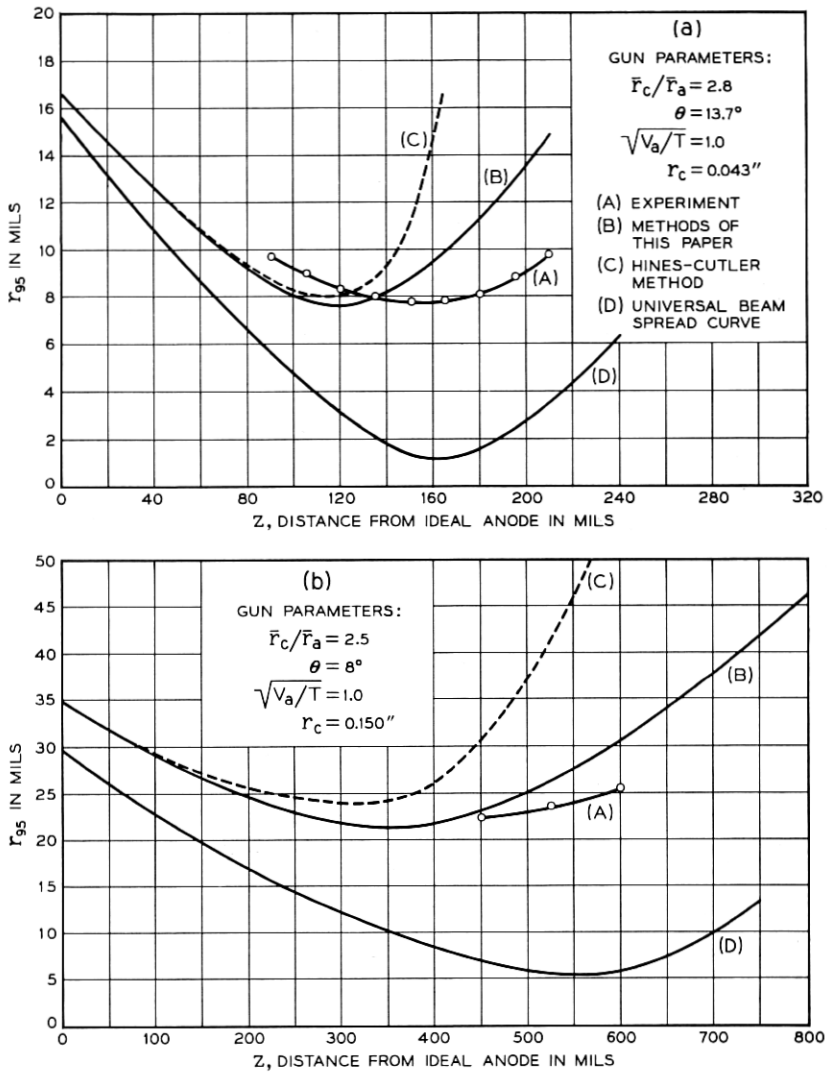

Fig. 15 — Beam profiles (using an anode lens correction of $\Gamma = 1.1$ and the gun parameters indicated) as obtained (A) from experiment, (B) by the methods of this paper, (C) Hines-Cutler method, (D) by use of the universal beam spread curve.

universal beam spread curve[12] (i.e., under the assumption of laminar flow and gradual variations of beam radius with distance). Note that in each case a value of 1.1 has been used for the correction factor, Γ, representing the excess divergence of the anode lens. The agreement in $(r_{95})_{min}$ as obtained from Curves A and B is remarkably good, but the axial position of $(r_{95})_{min}$ in Curve A definitely lies beyond the correspond-

ing minimum position in Curve B. Fortunately, in the gun design stage, one is usually more concerned with the value of $(r_{95})_{\min}$ than with its exact axial location. The principal need for knowing the axial location of the minimum is to enable the axial magnetic field to build up suddenly in this neighborhood. However, since this field is normally adjusted experimentally to produce best focusing, an approximate knowledge of $z_{\min}$ is usually adequate.

In Fig. 15b we show a similar set of experimental and theoretical beam profiles for another gun. The relative profiles are much the same as in Fig 15a, and all of several other guns measured yield experimental points similarly situated with respect to curves of Type B.

C. Comparison of Experimental and Theoretical Current Density Distributions where the Minimum Beam Diameter is Reached

In Fig. 14 we have plotted the current density distribution we would have predicted in a transverse plane at $z_{\min}$ for the example introduced in Section 5*D*. Here the experimental and theoretical curves are normalized to include the same total currents in their respective beams. The noticeable difference in predicted and measured current densities at the center of the beam does not appreciably alter the properties such a beam would have on entering a magnetic field because so little total current is actually represented by this central peak.

D. Variation of Beam Profile with Γ

All of the design charts have been based on a value of $\Gamma = 1.1$, which is typical of the values obtained by the methods of Section 3. When appreciably different values of Γ are appropriate, we can get some feeling for the errors involved, in using curves based on $\Gamma = 1.1$, by reference to Fig. 16. Here we show beam profiles as obtained by the methods of this paper for three values of Γ. The calculations are again based on the gun of Section 5*D*, and a value of just over 1.1 for Γ gives the experimentally obtained value for $(r_{95})_{\min}$.

7. SOME ADDITIONAL REMARKS ON GUN DESIGN

In previous sections we have not differentiated between the voltage on the accelerating anode of the gun and the final beam voltage. It is important, however, that the separate functions of these two voltages be kept clearly in mind: The accelerating anode determines the total current drawn and largely controls the shaping of the beam; the final beam voltage is, on the other hand, chosen to give maximum interaction between the electron beam and the electromagnetic waves traveling along the slow wave circuit. As a consequence of this separation of func-

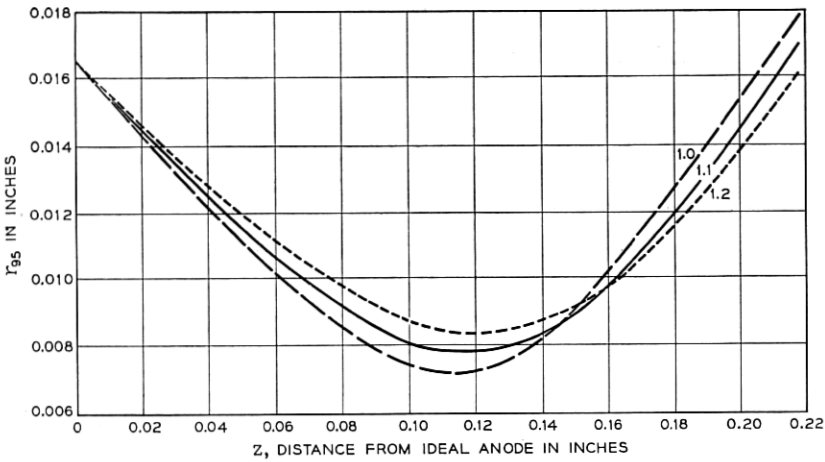

Fig. 16 — Beam profiles as obtained by the methods of this paper for the gun parameters given in Section 5*D*. Curves are shown for three values of the anode lens correction, viz. $\Gamma = 1.0$, 1.1, and 1.2.

tions, it is found that some beams which are difficult or impossible to obtain with a single Pierce-gun acceleration to final beam voltage may be obtained more easily by using a lower voltage on the gun anode. The acceleration to final beam voltage is then accomplished after the beam has entered a region of axial magnetic field.

Suppose, for example, that one wishes to produce a 2-ma, 4-kv beam with $(r_{95}/r_c) = 0.25$. If the cathode temperature is 1000°K, and the gun anode is placed at a final beam voltage of 4 kv, we have $\sqrt{V_a/T} = 2$ and $P = 0.008$. From the top set of curves under $\sqrt{V_a/T} = 2$ in Fig. 13, we find (by using a fairly crude extrapolation from the curves shown) that a ratio of $\bar{r}_c/\bar{r}_a \approx 3.5$ is required to produce such a beam. The value of (r_e/σ) at $z_{\min}$ is therefore less than about 0.2 so that there is little semblance of laminar flow here. On the other hand we might choose $V_z = 250$ volts so that $\sqrt{V_a/T} = 0.5$ and $P = 0.51$. From Fig. 13 we than obtain $\bar{r}_c/\bar{r}_a = 2.6$ and $(r_e/\sigma)_{\min} = 0.8$ for the same ratio of $r_{95}/r_c (= 0.25)$. While the flow could still hardly be called laminar, it is considerably more ordered than in the preceding case. Here we have included no correction for the (convergent) lens effect associated with the post-anode acceleration to the final beam voltage, $V = 4$ kv.

Calculations of the Hines-Cutler type will always predict, for a given set of gun parameters and a specified anode lens correction, a minimum beam size which is larger than that predicted by the methods of this paper. Nevertheless, in many cases the difference between the minimum sizes predicted by the two theories is negligible so long as the same anode lens correction is used. The extent to which the two theories agree ob-

viously depends on the magnitude of r_e/σ. When r_e/σ as calculated by the Hines-Cutler method (with a lens correction added) remains greater than about 2 throughout the range of interest, the difference between the corresponding values obtained for r_{95} will be only a few per cent. For these cases where r_e/σ does not get too small, the principal advantages of this paper are in the inclusion of a correction to the anode lens formula and in the comparative ease with which design parameters may be obtained. In other cases r_e/σ may become less than 1, and the theory presented in this paper has extended the basic Hines-Cutler approach so that one may make realistic predictions even under these less ideal conditions where the departure from a laminar-type flow is quite severe.

ACKNOWLEDGMENT

We wish to thank members of the Mathematical Department at B.T.L., particularly H. T. O'Neil and Mrs. L. R. Lee, for their help in programming the problem on the analog computer and in obtaining the large amount of computer data involved. In addition, we wish to thank J. C. Irwin for his help in the electrolytic tank work and both Mr. Irwin and W. A. L. Warne for their work on the beam analyzer.

REFERENCES

1. Pierce, J. R., Rectilinear Flow in Beams, J. App. Phys., **11,** pp. 548–554, Aug., 1940.
2. Samuel, A. L., Some Notes on the Design of Electron Guns, Proc. I.R.E., **33,** pp. 233–241, April, 1945.
3. Field, L. M., High Current Electron Guns, Rev. Mod. Phys., **18,** pp. 353–361, July, 1946.
4. Davisson, C. J., and Calbick, C. J., Electron Lenses, Phys. Rev., **42,** p. 580, Nov., 1932.
5. Helm, R., Spangenburg, K., and Field, L. M., Cathode-Design Procedure for Electron Beam Tubes, Elec. Comm., **24,** pp. 101–107, March, 1947.
6. Cutler, C. C., and Hines, M. E., Thermal Velocity Effects in Electron Guns, Proc. I.R.E., **43,** pp. 307–314, March, 1955.
7. Cutler, C. C., and Saloom, J. A., Pin-hole Camera Investigation of Electron Beams, Proc. I.R.E., **43,** pp. 299–306, March, 1955.
8. Hines, M. E., Manuscript in preparation.
9. Private communication.
10. See for example, Zworykin, V. K., et al., Electron Optics and the Electron Microscope, Chapter 13, Wiley and Sons, 1945, or Klemperer, O., Electron Optics, Chapter 4, Cambridge Univ. Press, 1953.
11. Brown, K. L., and Süsskind, C., The Effect of the Anode Aperature on Potential Distribution in a "Pierce" Electron Gun, Proc. I.R.E., **42,** p. 598, March, 1954.
12. See, for example, Pierce, J. R., Theory and Design of Electron Beams, p. 147, Van Nostrand Co., 1949.
13. See Reference 6, p. 5.
14. Langmuir, I. L., and Blodgett, K., Currents Limited by Space Charge Between Concentric Spheres, Phys. Rev., **24,** p. 53, July, 1924.
15. See Reference 12, p. 177.
16. See Reference 12, Chap. X.